Title
The Mechanosensitive Ion Channel Piezo Inhibits Axon Regeneration

Journal
Neuron, 102(2)

ISSN
0896-6273

Authors
Song, Yuanquan
Li, Dan
Farrelly, Olivia
et al.

Publication Date
2019-04-01

DOI
10.1016/j.neuron.2019.01.050

Peer reviewed

HHS Public Access

Author manuscript

Neuron. Author manuscript; available in PMC 2019 April 29.

Published in final edited form as:

Neuron. 2019 April 17; 102(2): 373–389.e6. doi:10.1016/j.neuron.2019.01.050.

The Mechanosensitive Ion Channel Piezo Inhibits Axon Regeneration

Yuanquan Song[1,2,*], **Dan Li**[1,2,11], **Olivia Farrelly**[3,11], **Leann Miles**[4,11], **Feng Li**[1,2], **Sung Eun Kim**[5,6], **Tsz Y. Lo**[1], **Fei Wang**[7], **Tun Li**[5,6], **Katherine L. Thompson-Peer**[5,6], **Jiaxin Gong**[7], **Swetha E. Murthy**[8], **Bertrand Coste**[8,10], **Nikita Yakubovich**[9], **Ardem Patapoutian**[8], **Yang Xiang**[7], **Panteleimon Rompolas**[3], **Lily Yeh Jan**[5,6,9], and **Yuh Nung Jan**[5,6,9,12,*]

[1]Raymond G. Perelman Center for Cellular and Molecular Therapeutics, The Children's Hospital of Philadelphia, Philadelphia, PA 19104, USA

[2]Department of Pathology and Laboratory Medicine, University of Pennsylvania, Philadelphia, PA 19104, USA

[3]Department of Dermatology, University of Pennsylvania, Philadelphia, PA 19104, USA

[4]The Graduate Group in Biochemistry and Molecular Biophysics, University of Pennsylvania, Philadelphia, PA 19104, USA

[5]Departments of Physiology, Howard Hughes Medical Institute, University of California, San Francisco, San Francisco, CA 94158, USA

[6]Howard Hughes Medical Institute, University of California, San Francisco, San Francisco, CA 94158, USA

[7]Department of Neurobiology, University of Massachusetts Medical School, Worcester, MA 01605, USA

[8]Department of Neuroscience, The Scripps Research Institute, Howard Hughes Medical Institute, La Jolla, CA 92037, USA

[9]Department of Biochemistry and Biophysics, University of California, San Francisco, San Francisco, CA 94158, USA

[10]Present address: Aix Marseille Université, CNRS, LNC-UMR 7291, 13344 Marseille, France

[11]These authors contributed equally

[12]Lead Contact

[*]Correspondence: songy2@email.chop.edu (Y.S.), yuhnung.jan@ucsf.edu (Y.N.J.).

AUTHOR CONTRIBUTIONS

Conceptualization, Y.S., D.L., S.E.K., and Y.N.J.; Methodology, Y.S., D.L., and P.R.; Investigation, Y.S., D.L., O.F., L.M., F.L., T.L., T.Y.L., K.L.T.-P., S.E.M., and B.C.; Formal Analysis, F.W. and Y.X.; Writing – Original Draft, Y.S., Y.N.J., and L.Y.J.; Writing – Review & Editing, P.R., Y.X., and A.P.; Funding Acquisition, Y.S., Y.N.J., and L.Y.J.; Resources, J.G. and N.Y.; Supervision, Y.S., P.R., and Y.N.J.

SUPPLEMENTAL INFORMATION

Supplemental Information can be found with this article online at https://doi.org/10.1016/j.neuron.2019.01.050.

DECLARATION OF INTERESTS

The authors declare no competing interests.

SUMMARY

Neurons exhibit a limited ability of repair. Given that mechanical forces affect neuronal outgrowth, it is important to investigate whether mechanosensitive ion channels may regulate axon regeneration. Here, we show that DmPiezo, a Ca^{2+}-permeable non-selective cation channel, functions as an intrinsic inhibitor for axon regeneration in *Drosophila*. DmPiezo activation during axon regeneration induces local Ca^{2+} transients at the growth cone, leading to activation of nitric oxide synthase and the downstream cGMP kinase Foraging or PKG to restrict axon re-growth. Loss of DmPiezo enhances axon regeneration of sensory neurons in the peripheral and CNS. Conditional knockout of its mammalian homolog Piezo1 *in vivo* accelerates regeneration, while its pharmacological activation *in vitro* modestly reduces regeneration, suggesting the role of Piezo in inhibiting regeneration may be evolutionarily conserved. These findings provide a precedent for the involvement of mechanosensitive channels in axon regeneration and add a potential target for modulating nervous system repair.

In Brief

Piezo is a mechanosensitive ion channel that transduces mechanical stimuli into cellular responses. Here, Song et al. show that Piezo is recruited after axon injury to inhibit axon regeneration via the CamKIINos-PKG pathway, a process that may be evolutionarily conserved.

INTRODUCTION

Neurons and other types of cells are exposed to mechanical forces generated intracellularly, for example, via molecular motors and microtubule dynamics, and/or through interactions with the extracellular environment (Franze et al., 2013; Jaalouk and Lammerding, 2009; Suter and Miller, 2011), including adhe sive tension between neurons and substrates during neuronal development, morphogenesis, and circuit formation (Franze et al., 2013; Jaalouk and Lammerding, 2009). Mechanical forces may affect neuronal outgrowth, for example, stretching a growth cone of a cultured chick or rat sensory ganglion neuron leads to extensive elongation of the axon (Bray, 1984; Lamoureux et al., 1989; Pfister et al., 2004; Suter and Miller, 2011). This stretch-induced axonal elongation also occurs in human sensory neurons, rat PC12 cells, and *Aplysia* neurons (Smith, 2009; Suter and Miller, 2011). The elongated axons maintain their thickness and propagate action potentials, suggesting that stretch activates protein synthesis and transport pathways (Pfister et al., 2006). However, little is known about the underlying molecular and cellular machinery.

In mechanosensory neurons, mechanical stimuli activate mechanosensitive (MS) ion channels that permeate cations (Nilius and Honoré, 2012) to transmit signals such as touch and sound, and to mediate processes such as blood pressure regulation (Chalfie, 2009). Eukaryotic mechanosensitive cation channels identified thus far include Piezo and NompC (Coste et al., 2012; Kim et al., 2012; Yan et al., 2013). *In vitro* studies suggest a role of mechanosensitive ion channels in neuronal outgrowth for cultured *Xenopus* spinal neurons (Jacques-Fricke et al., 2006) and rat PC12 cells (Gottlieb et al., 2010), as well as in mediating transient calcium influx, in part through TRPC1 at the growth cones to regulate neurite extension (Kerstein et al., 2013). It will be of interest to determine how endogenous

mechanosensitive ion channels may regulate neurite outgrowth, and whether they also regulate regeneration. In this study, we show that the mechanosensitive cation channel Piezo functions in *Drosophila* sensory and motor neurons, and possibly also in rodent sensory and central neurons to inhibit axon regeneration. We further delineate the Piezo-CamKII-Nos-PKG signaling pathway, which underlies the response after neuronal injury for the regulation of axon regeneration in *Drosophila*. Moreover, we have developed a new mouse sensory neuron injury model—the corneal sensory nerve laser ablation model, which allows *in vivo* live imaging of sensory axon regeneration in mammals.

RESULTS

Piezo Inhibits Axon Regeneration

To study axon regeneration, we used the *Drosophila* dendritic arborization (da) sensory neuron injury model (Song et al., 2012, 2015). With a two-photon laser, we severed the axon of mechanosensitive class III da neurons (labeled with *19–12-Gal4 > CD4tdGFP, repo-Gal80*) in the peripheral nervous system (PNS) of 2nd-instar larvae at 48 hr after egg laying (hr AEL), confirmed the degeneration of the distal axon after one day (at 72 hr AEL) and assessed its regeneration after 2 more days (120 hr AEL) (Figure 1A). In contrast to wild-type (WT) class III da neurons that failed to regenerate axons (Figure 1A, arrow), in a null mutant of *Drosophila* Piezo *DmPiezoKO*, new axons regrew from the retracted axon stem and extended along the original trajectory, way beyond the injury site (Figure 1A, arrowheads). The function of *DmPiezo* is cell autonomous because its RNAi knockdown in class III da neurons (*19–12-Gal4 > DmPiezo RNAiv2796*) recapitulated the enhancement of regeneration. Moreover, expression of DmPiezo in class III da neurons of *DmPiezoKO* mutants (*DmPiezoKO*; *19–12-Gal4>DmPiezo*) suppressed the mutant phenotype (Figure 1A). The regeneration phenotype was further quantified by assessing the “regeneration percentage” and “regeneration index” (Figures 1B–1D and S1A–S1C; STAR Methods), as described previously (Song et al., 2012). Unlike regeneration index, the regeneration length without normalization represents raw data that reflect scaling and axon regeneration in a larva that continues to grow during the course of the experiment. The regeneration parameters from various genotypes were compared to that of the WT if not noted otherwise, and only those with significant difference were labeled with the asterisks.

To ask whether the function of Piezo in inhibiting axon regeneration is evolutionarily conserved, we first expressed its mammalian homologs in class III da neurons of *DmPiezoKO* mutants. We also tested their role in mammalian axon regeneration (see below). Both mouse Piezo1 (mPiezo1) and human Piezo1 (hPiezo1) could substitute for DmPiezo and suppress the enhancement of regeneration phenotype of *DmPiezoKO* mutants (Figures 1B–1D, S1B, and S1C), suggesting that the ability of Piezo to inhibit axon regeneration may be evolutionarily conserved. To test the requirement of the channel activity, we expressed a mutant mPiezo1, which contains a Myc tag insertion in the last extracellular loop mPeizo1–2336-Myc, rendering the channel non-functional without affecting its expression or trafficking to the membrane (Chen et al., 2018; Coste et al., 2015), in class III da neurons of *DmPiezoKO* mutants. In contrast to mPiezo1, mPiezo1–2336-Myc failed to suppress the increased regeneration phenotype (Figures 1B–1D, S1B, and S1C),

indicating that the mechano-sensitive ion channel function of Piezo is essential for its role as a regeneration inhibitor.

To test whether overexpression of Piezo in neurons normally capable of regeneration will reduce their regenerative potential, we focused on class IV da neurons. Unlike class III da neurons, class IV da neurons are capable of regenerating its axon (Song et al., 2015). We labeled class IV da neuron with *ppk-CD4tdGFP* and used the following injury protocol: axotomy was induced at 72 hr AEL, degeneration was confirmed at 96 hr AEL and regeneration was assayed at 120 hr AEL (Song et al., 2015). Compared to WT class IV da neurons, which exhibited axon regeneration about 75% of the time, overexpression of WT DmPiezo in class IV da neurons did not alter regeneration (Figures 1E–1G). We next tested whether overexpression of a Piezo1 gain-of-function variant can alter regeneration. Various mutations in human Piezo1 that prolong channel opening by slowing inactivation cause dehydrated hereditary stomatocytosis (Albuisson et al., 2013; Andolfo et al., 2013; Bae et al., 2013). In our structure-function analysis of Piezo1, we discovered a triple mutant of mPiezo1 mPiezo1-TriM (E2133D + D2139E + D2144E), which when expressed in HEK293T cells resulted in a mechanically activated current that inactivated very slowly, both in the whole-cell patch configuration (14-fold relative to WT) and cell-attached configuration (3.6-fold relative to WT) (Figures S1D–S1F) (Coste et al., 2015). Quantitatively, the effect of these mutations on inactivation was more severe than any of the human Piezo1 mutants previously described (Albuisson et al., 2013; Bae et al., 2013). Strikingly, overexpression of the mPiezo1-TriM gain-of-function mutant in class IV da neurons reduced the regeneration percentage to 48% and decreased the length of the regrown axons (Figures 1E–1G). This observation further supports the hypothesis that the mechanosensitive ion channel function of Piezo is critical for its ability to inhibit axon regeneration.

To address whether removing Piezo is beneficial for axon regeneration in the CNS, we examined class IV da neuron axon regeneration within the ventral nerve cord (VNC) after CNS lesion, as previously described (Song et al., 2015). Compared to WT control, which showed limited regrowth, *DmPiezoKO* improved the regeneration percentage, with a moderate increase in “terminal branching” and “commissure regrowth” (Figures 2A–2C; STAR Methods). The enhancement of regeneration is unlikely to be due to developmental defects of axon outgrowth, because the patterning in the uncut VNC appears normal for class IV and class III da neuron axons, for all axons labeled by Fas II staining (Figures S2A–S2C) and for class III da neuron axon terminals (Figure S2D).

DmPiezo inhibited axon regeneration of not only sensory neurons but also motor neurons. Loss of DmPiezo function in motor neurons also promoted motor axon regeneration after nerve crush, as evident from the increased elaboration of growth cones (Figures S2E and S2F; STAR Methods).

To test whether DmPiezo also affects dendrite regeneration, we examined dendrite regeneration in class III da neurons using two injury paradigms: lesioning a single dendrite (Song et al., 2012) versus removing all dendrites—balding (Stone et al., 2014). After single-dendrite injury, both WT and *DmPiezoKO* showed limited regeneration, as indicated by the

regeneration percentage and the number of dendritic branches added (Figures 2E and 2F). On the other hand, after balding, both WT and *DmPiezoKO* showed substantial regeneration, but no further enhancement was seen after removing *DmPiezo* (Figures 2D, 2E, and 2G). Therefore, Piezo exhibits a specific role in regulating axon but not dendrite regeneration.

We found expression of DmPiezo in both class III and class IV da neurons based on two experiments. First, the *DmPiezo-Gal4>CD4tdTomato* reporter is expressed in class III da neurons that are marked by *NompC-QF>mCD8GFP* (Figure S2G, arrowheads). *DmPiezo-Gal4>CD4tdTomato* is also present in class IV da neurons (Figure S2G, arrow), as reported previously (Kim et al., 2012). Second, we generated a GFP-DmPiezo knockin fly by fusing GFP with the N terminus of the DmPiezo protein using the CRISPR technology to examine the endogenous DmPiezo expression pattern. Given that GFP-DmPiezo overexpression in class IV da neurons rescues the defects in sensing harsh touch in *DmPiezoKO* (Kim et al., 2012), we expect that N-terminal GFP tagging of DmPiezo should not disrupt DmPiezo function. We found that without injury, GFP-DmPiezo is present diffusely in the class III da neuron cell body and axon, as labeled with *NompC-QF>mtdTomato* (Figure 1H). Notably, GFP-DmPiezo appears to be enriched in the growth cone tip 24 hr after axon injury (Figure 1H), revealing that the spatiotemporal expression of Piezo is consistent with its role in inhibiting regeneration.

To test whether Piezo functions specifically during regeneration, we utilized an inducible system that offers temporal control of gene expression by regulating temperature—$Gal80^{ts}$, a temperature-sensitive suppressor of Gal4 (McGuire et al., 2003). Under the permissive temperature, $Gal80^{ts}$ effectively shuts off Gal4 expression. When shifted to the restrictive temperature, $Gal80^{ts}$ is misfolded, leading to Gal4 expression. Accordingly, we raised the larvae at 25°C until injury and then shifted to 30°C to allow *DmPiezo RNAi* expression. Class III da neurons were labeled by *NompC-QF>mCD8GFP* and the RNAi was expressed by *19–12-Gal4*, *UAS-CD4tdGFP*, *repo-Gal80* under the suppression of the ubiquitous *tub-*$Gal80^{ts}$ (Figure 3), thus enabling knockdown of *DmPiezo* specifically after injury or during regeneration. We first determined the induction efficiency of Gal4 upon the shift to 30°C, using GFP as the reporter (Figure S3A). While no GFP^+ neurons were detectable at 12 hr after induction, we found GFP expression in about 35% of class III da neurons at 24 hr, and ~70% of class III da neurons at 72 hr (Figure S3A, arrows). By inducing *DmPiezo RNAi* immediately after injury, we showed that the restricted removal of DmPiezo is sufficient to enhance class III da neuron axon regeneration (Figure 3), indicating that Piezo acts after injury to specifically affect regeneration.

Piezo Functions through Calcium Signaling to Inhibit Axon Regeneration

What might be the function of DmPiezo in class III da neurons? As shown previously (Yan et al., 2013), WT class III da neurons in abdominal segments of fillet preparations displayed increased firing of action potentials (APs) in response to progressively larger displacements of the larval body wall (Figure 4A, black solid circles), a response that largely depends on NompC (Yan et al., 2013) but not on DmPiezo (Figure 4A). As expected, no significant difference was detected in *DmPiezoKO* (Figure 4A, red circles). This response to

mechanical stimuli was largely abolished after injury of the axon (Figure 4A, black and red open circles), possibly due to injury-induced atrophy.

We found that axon lesion triggered an immediate burst of action potentials of comparable frequency and duration in both WT and *DmPiezoKO* (Figure 4B), suggesting that the action of Piezo in regeneration may not be at the level of neuronal excitability directly triggered by the axon injury per se. Alternatively, Piezo channels could be activated during axon regrowth, by the mechanical force derived from the interaction between the growth cone or filopodia and the surrounding environment. Given that Piezo is a cationic channel with Ca^{2+} permeability (Figure S3B), we went on to perform calcium imaging in class III da neuron axons and growth cones, to assess Piezo channel activity. Before injury (pre-injury), class III da neurons exhibited spontaneous calcium spikes in the proximal axon in both WT and *DmPiezoKO* (Figures 4E, S4A, and S4B; Videos S1 and S2). At 24 hr after injury (AI), a stage when axon degeneration is mostly complete but extensive regeneration has not taken place, both WT and *DmPiezoKO* showed similar spontaneous calcium transients in the growth cone. However, the amplitude was smaller than that of the pre-injury condition (Figures 4F, S4C, and S4D; Videos S3 and S4). Most importantly, at 48 and 72 hr AI, amid robust axon regeneration in *DmPiezoKO*, spontaneous calcium transients were readily detected in the growth cones and filopodia in WT, but the signal was much attenuated in *DmPiezoKO* (Figures 4C, 4D, 4G, and S4E; Videos S5 and S6). Interestingly, we were able to occasionally capture the filopodia dynamics and observed that calcium spikes preceded filopodia retraction (3 neurons and 4 filopodia out of 33 neurons imaged; Video S5, arrow). These data suggest that Piezo channels are likely activated when the reformed growth cone is actively exploring and interacting with the environment such as glial cells, and that the reduced calcium transients correlate with enhanced axon regeneration in Piezo knockout animals.

In order to dissect the Piezo-induced calcium signaling in regulating regeneration, we first focused on a critical regulator of the calcium signaling pathway—Ca^{2+}/calmodulin-dependent protein kinase II (CamKII). Inhibiting CamKII activity specifically in class III da neurons by overexpressing either the inhibitory peptide CamKII-I.Ala (Joiner and Griffith, 1997) or CamKII RNAi (Ashraf et al., 2006) led to substantial axon regeneration, to a similar extent as seen in *DmPiezoKO* (Figures 5A–5D). Suppressing CamKII activity in the absence of DmPiezo did not trigger a stronger regenerative response, as compared to *DmPiezoKO* alone (Figures 5A–5D). Moreover, overexpression of the constitutively active CamKII.T287D (Park et al., 2002) in the *DmPiezoKO* background attenuated the enhanced regeneration phenotype, consistent with CamKII as a downstream effector of Piezo in inhibiting regeneration. We then went on to determine the genetic interaction between DmPiezo and Calmodulin, a calcium-binding messenger protein. While axon regeneration is slightly improved in the $Cam^{n339/+}$ heterozygotes for a Calmodulin-null allele, transheterozygotes of $Cam^{n339/+}$ and $DmPiezoKO^{/+}$ significantly promote axon regeneration (Figures 5A and 5E–5G), confirming that DmPiezo and Calmodulin function in the same genetic pathway.

Besides genetic analyses, we further investigated the calcium signaling pathway, by analyzing the phosphorylation status of CamKII with the phospho-CaMKII (Thr^{305})

antibody. Ca^{2+}/CaM binding activates CamKII and binding of two Ca^{2+}/CaM molecules stimulates the phosphorylation of Thr^{286} (Thr^{287} in flies), leading to maximal activity. Once Ca^{2+}/CaM dissociates, the enzyme remains active but at a lower level. The dissociation of Ca^{2+}/CaM exposes Thr^{305} and Thr^{306} (Thr^{306} and Thr^{307} in flies), which rapidly become autophosphorylated. Therefore, Thr^{305} (Thr^{306} in flies) phosphorylation corresponds to a state that is reached after attaining peak activity but prior to reactivation (Griffith, 2004). We first verified the specificity of the antibody, as CamKII RNAi in class III da neurons specifically abolished the phosphor-CamKII (Thr^{305}) staining in the cell body, dendrites, and axon (Figure 5I). We then analyzed the staining pattern before injury, 24 hr AI, and 48 hr AI. Prior to injury, phosphor-CamKII (Thr^{305}) staining was present in the class III da neuron cell body and diffusely in the axon and dendrites, both in WT and *DmPiezoKO* (Figure 5H). At 24 hr AI, a small fraction (14%) of the injured class III da neurons in WT or *DmPiezoKO* showed staining in the growth cone tip (Figure 5J). Notably, at 48 h AI, phosphor-CamKII (Thr^{305}) staining was detected in the growth cone tip of 50% of the WT class III da neurons but not in *DmPiezoKO* class III da neurons (Figures 5H and 5J, arrow), suggesting that CamKII responds to axon injury and/or regeneration in a Piezo-dependent manner. These data further suggest that Piezo and CamKII and Cam function in the same pathway, and that Piezo activation induced AI is likely transduced through calcium signaling to downstream effectors.

NO Signaling Functions Downstream of Piezo in Inhibiting Axon Regeneration

To further probe the machinery downstream of Piezo, we focused on nitric oxide synthase (NOS), a central regulator of NO signaling, for two reasons. First, mPiezo1 activity drives endothelial cell migration via endothelial NOS during mammalian vasculature development (Li et al., 2014). Second, NOS activity is known to be Ca^{2+}/Calmodulin dependent (Marletta, 1994; Nathan and Xie, 1994; Regulski and Tully, 1995). With two Nos-null alleles, $Nos^{\Delta 15}$ and Nos^{1}, we found that both $Nos^{\Delta 15}$ (Figure 6) and transheterozygotes of $Nos^{\Delta 15}/Nos^{1}$ (Figures S5A–S5D) resulted in enhanced axon regeneration, similar to that of *DmPiezoKO*, and expression of Nos specifically in class III da neurons was sufficient to rescue the phenotype of $Nos^{\Delta 15}$ (Figures S5A–S5D). Moreover, overexpression of Nos (two copies of *UAS-Nos*) in class IV da neurons significantly reduced their regeneration potential (Figures S5E–S5G), lending further support to the notion that Nos is an intrinsic inhibitor for axon regeneration.

To assess the genetic interaction between *DmPiezo* and *Nos*, we examined transheterozygotes and carried out epistasis analysis. While heterozygotes of $DmPiezoKO/^{+}$ and $Nos^{\Delta 15}/^{+}$ behaved similarly as the WT control, the transheterozygotes $DmPiezoKO/^{+}$, $Nos^{\Delta 15}/^{+}$ resembled *DmPiezoKO* and $Nos^{\Delta 15}$ (Figures 6A–6D), suggesting they function in the same pathway. Moreover, overexpression of Nos in class III da neurons in *DmPiezoKO* was sufficient to suppress the enhanced regeneration phenotype, consistent with the model that Nos lies downstream of Piezo in inhibiting axon regeneration.

In addition, similar to the effect of *DmPiezoKO*, loss of Nos function in $Nos^{\Delta 15}$ mutants enhanced class IV da neuron axon regeneration in the CNS (Figure S6A), with a modest increase in regeneration percentage and commissure regrowth (Figures S6B and S6C).

for or PKG Inhibits Axon Regeneration Downstream of Nos

Given the possibility that Nos lies downstream of Piezo, we wondered how Nos might relay the signal from Piezo activation to restrict axon regeneration. Recognizing the important role of the second messenger cGMP in NO signaling, we tested for the involvement of the cGMP-dependent kinase Foraging, dg2, or PKG in axon regeneration. The *foraging* (*for*) locus produces 11 transcripts encoding four protein isoforms (Davies, 2006), among which nine encode the three major FOR protein isoforms FOR-T1, T2, and T3 (Figure S7A) (Eddison et al., 2012). We found that class III da neuron axon regeneration was significantly boosted in a mutant allele of *for* $for^{k047037}$ (Figures 7A–7D), an allele with a P-element inserted in the intron, disrupting mRNA splicing and reducing transcript expression of the *for-T1* and *T3* isoforms (Figures S7A and S7B). This phenotype was confirmed in transheterozygotes of $for^{k047037}$ over a deficiency line $for^{DfED243}$ that removes the first few exons of *for-T1*/*T3*, and the promoter region of *for-T2* (Figures 7A–7D and S7A). The function of *for* is required cell autonomously as class III da neuron-specific knockdown of *for* with RNAi targeting all *for* isoforms (Figure S7A) was sufficient to phenocopy the regeneration enhancement (Figures 7A–7D). On the other hand, no obvious phenotype was detected in $for^{11.247}$, which carries a P element insertion in the 5′ region of the *for* locus (Figures 7B–7D and S7A), suggesting likely compensations among *for* isoforms in regulating regeneration.

Next, we tested the effectiveness of various *for* isoforms in inhibiting axon regeneration when overexpressed in class IV da neurons. Although expressing a single copy of FOR-T1 with two independent alleles: *for-T1* and *dg2-P1* or FOR-T2 with *dg2-P2A* failed to achieve significant inhibition, overexpressing two copies of FOR-T1 (*for-T1X2*) dramatically impeded axon regeneration (Figures 7E–7G). These data demonstrate that *for* functions as a brake for axon regeneration, and that its effect is dosage dependent.

Next, we went on to determine the genetic interaction between *Nos* and *for*. Whereas heterozygotes of $Nos^{\Delta 15/+}$ or $for^{k047037/+}$ behaved similarly as WT control, transheterozygotes of $Nos^{\Delta 15/+}$ and $for^{DfED243/+}$ displayed enhanced class III da neuron axon regeneration resembling that of $Nos^{\Delta 15}$ and *DmPiezoKO* (Figures 7A and 7H–7J), suggesting that they function in the same pathway. Moreover, overexpression of Nos in class III da neurons failed to mitigate the regeneration enhancement seen in $for^{k047037}$, whereas FOR-T1 overexpression largely sup pressed the phenotype in $Nos^{\Delta 15}$ (Figures 7A and 7K–7M), suggesting that *for* acts as a downstream effector for Piezo and Nos in inhibiting axon regeneration.

Piezo-Mediated Inhibition of Axon Regeneration in Mammals

The function of Piezo in mechanosensation is conserved from fly to mammals (Coste et al., 2010; Kim et al., 2012). Having found that mPiezo1 and hPiezo1, like DmPiezo, suppressed the enhanced axon regeneration phenotype in *DmPiezoKO*, and that the mPiezo1-TriM mutant inhibited axon regeneration in flies, we hypothesize that Piezo1 may also function as a regeneration inhibitor in mammals. We tested this hypothesis using injury models in cultured neurons and in mice *in vivo*.

First, we adopted an *in vitro* axotomy paradigm based on a microfluidic device (Zhou et al., 2016). Briefly, we cultured rat hippocampal neurons in a microfluidic chamber where neuronal cell bodies and dendrites are restricted to the soma chamber, while axons grow into the axon terminal chamber through long (450 mm in length) microgrooves. The axons in the terminal chamber were removed by vacuum aspiration at 7 days *in vitro* (DIV7) and axon regrowth was assessed 24 hr AI (Figure S8A). To activate Piezo1, we applied the Piezo1 agonist Yoda1 (30 mM) (Syeda et al., 2015) to the terminal chamber immediately after axotomy. We found that Piezo1 activation modestly reduces the axon regrowth capacity (Figure 8A). Regrown axon coverage areas (Figure S8B; STAR Methods) are modestly but significantly decreased in the Yoda1-treated neurons as compared to the DMSO vehicle control (Figure 8B). Thus, activating mammalian Piezo1 also attenuates axon regeneration AI.

To analyze axon regeneration *in vivo* in mice in real time, we developed a novel injury model based on laser axotomy of corneal sensory nerves. The cornea is highly innervated by sensory neurons that are derived from the ophthalmic division of the trigeminal nerve (Müller et al., 2003). Within the corneal stroma, nerve bundles separate into smaller processes that extend centripetally to form the subbasal nerve plexus (Müller et al., 1996; Schimmelpfennig, 1982). To label corneal sensory axons and generate sensory neuron-specific Piezo1 conditional knockout (*Piezo1 cKO*), we bred mice with *Advillin-CreER; Rosa-stop-tdTomato; Piezo1*$^{fl/fl}$ alleles and induced Cre mediated recombination with tamoxifen (TAM) injection (Figure 8D; STAR Methods). To visualize and manipulate tdTomato-labeled corneal sensory nerves in live mice we took advantage of the accessibility of the eye and adapted a previously developed intravital imaging system based on 2-photon microscopy (Huang and Rompolas, 2017; Rompolas et al., 2012). Using a femtosecond pulsed laser, we ablated the larger nerve trunks located in the stroma before they branched into thinner fibers (Figure 8F). Serial optical sections of the entire cornea were collected immediately before (day 0) and at three time points after the ablation: day 2, day 4, and day 7 post-ablation (Figure 8E). We validated the degeneration of the nerve fibers downstream of the ablation sites both in the stroma and in the subbasal nerve plexus by imaging at 24 and 48 hr after ablation (Figure 8F). We did not observe gross anatomical defects in the patterning of corneal sensory nerves in the *Piezo1 cKO* prior to injury (Figure S8C). We found that in the control group (normal siblings), corneal sensory axons displayed signs of regeneration within 4 days post-ablation, while limited regrowth was achieved at day 7 post-ablation, leaving large areas deprived of sensory innervation (Figures 8G and S8C). On the other hand, in *Piezo1 cKO*, acceleration of axon regeneration was observed at day 4 and day 7 post-ablation. A larger area of the vacant space was reinnervated by the regenerating nerve fibers (Figures 8G and S8C). The regenerating axons were manually traced and the length of regrown axons was measured (Figure S8D; STAR Methods). *Piezo1 cKO* exhibited significantly higher regeneration capacity as reflected by the increase of the total length of regenerating nerve fibers (Figures 8H and S8E). These results suggest that Piezo1 may also function intrinsically in neurons to inhibit axon regeneration in mammals, a process that may be evolutionarily conserved.

DISCUSSION

Whereas the effect of mechanical forces on axon outgrowth was initially observed two decades ago, whether endogenous mechanosensitive ion channels regulate axon regeneration and, if so, what might be the underlying molecular mechanisms were unknown. We found that the mechanosensitive cation channel Piezo transduces the injury response to the NO signaling pathway through CamKII, with the cGMP-dependent kinase PKG as a downstream effector of NO synthase in *Drosophila* (Figure 8C). All components identified in this signaling cascade are intrinsically inhibitory to axon regeneration, providing potential targets for designing regeneration therapy. Ion channels are highly druggable targets, owing in large part to their localization to the plasma membrane. Our finding that inhibiting the Piezo channel promotes axon regeneration in fly and possibly also in mouse provides impetus for considering Piezo channel blockers as a potential means for promoting neural recovery.

Piezo proteins are pore-forming subunits of ion channels that open in response to mechanical stimuli, allowing cations, including calcium, to flow into the cell (Coste et al., 2010). Piezo orthologs are found in numerous eukaryotes (Wu et al., 2017). Most vertebrates have two isoforms, Piezo1 and Piezo2, whereas there is a single *Drosophila* ortholog (Coste et al., 2012; Kim et al., 2012). Piezo1 senses shear stress and mediates stretch-activated currents in flow-sensitive cells, such as red blood cells and vascular endothelial cells (Faucherre et al., 2014; Li et al., 2014; Ranade et al., 2014a). Piezo1 also senses the local cellular environment in neurons and other cells, thereby promoting downstream changes in cell-cell interactions, lineage choice, and motility (Blumenthal et al., 2014; Hung et al., 2016; Pathak et al., 2014). Piezo2 is primarily associated with sensory-specific roles, responding to light mechanical touch and mediating proprioception (Maksimovic et al., 2014; Ranade et al., 2014b; Woo et al., 2014, 2015). Intriguingly, while it was reported that morpholino knockdown of Piezo1 in *Xenopus* results in aberrant axonal growth and pathfinding errors (Koser et al., 2016), *Drosophila* DmPiezo knockout and mouse sensory neuron-specific conditional knockout display no obvious defects during developmental axon patterning or guidance but specifically exhibit enhanced axon regeneration AI. This may be attributed to the species difference or the different neuronal cell types analyzed. It is also possible that other mechanosensitive ion channels may compensate for the loss of DmPiezo in flies or Piezo1 in mouse. It will be of interest to examine the axon growth and regeneration phenotypes in mammals with both Piezo1 and Piezo2 removed from neurons. Importantly, Piezo1 is expressed at very low levels in sensory neurons in mice (Ranade et al., 2014b), consistent with our observation of the lack of gross developmental defects in sensory axons. In light of the axon regeneration phenotype we observed, these results suggest that, whereas normally Piezo1 may be expressed at very low basal level in sensory or hippocampal neurons, it may be locally redistributed or upregulated AI. Our results showing the enhanced axon regeneration in mammalian injury models present the first step toward understanding the potentially conserved role of Piezo in inhibiting neuroregeneration. Future studies are warranted to further substantiate and extend our observations, and to determine how this process is regulated, such as Piezo expression, distribution, and dynamics in response to injury.

In humans, mutations of PIEZO1 or PIEZO2 have been linked to several hereditary diseases, including dehydrated hereditary stomatocytosis (Albuisson et al., 2013; Andolfo et al., 2013; Bae et al., 2013; Beneteau et al., 2014; Shmukler et al., 2014; Zarychanski et al., 2012), distal arthrogryposis type 5 (Coste et al., 2013), Gordon syndrome and Marden-Walker syndrome (McMillin et al., 2014), displaying symptoms such as stiffness, impaired mobility of joints, and mental retardation. It will be intriguing to determine whether some of these symptoms may be attributed to neural circuit malformation, as a result of defective Piezo regulation on axon growth and/or maintenance and/or regeneration. Moreover, it is interesting to find that the TriM mutant of mPiezo1, but not the WT DmPiezo, is capable of reducing axon regeneration when overexpressed in class IV da neurons. We hypothesize that because mPiezo1-TriM shows over-activation of the channel, the same amount of force may elicit longer-lasting channel opening and calcium entry to amplify the downstream signaling, leading to inhibition of regeneration.

How might Piezo be activated upon neural injury? The sudden change of membrane tension after axon breakage may be sufficient to activate the channel. It is also conceivable that the extensive interaction among the damaged and/or regrowing axon, glial cells, and the extracellular matrix may contribute to channel activation. We found that the axon injury induced action potential firing is not altered, but there is a significant reduction of calcium transients, specifically in the growth cone, during active regeneration in the *DmPiezo* knockout. This favors the hypothesis that Piezo channels may be activated, re-localized, or upregulated during axon regeneration, as a result of the interaction between the growth cone and the local environment. We propose that the Piezo-dependent response to mechanical forces experienced by the growth cones leads to calcium influx that shuts down the regeneration program. This is reminiscent of a previous observation that suggests that Ca^{2+} influx through mechanosensitive ion channels at distinct microdomains in the growth cones inhibits axon outgrowth (Jacques-Fricke et al., 2006). Future studies to monitor the mechanical forces during injury and regeneration, using mechanosensitive reporters or atomic force microscopy (AFM), are warranted to test this hypothesis. Moreover, our finding is consistent with previous reports that calcium influx through voltage-gated calcium channels suppresses axon regeneration in the mammalian CNS (Enes et al., 2010; Tedeschi et al., 2016). Collectively, these studies suggest that the spatial and temporal arrangement of calcium signaling, especially acting through the CamKII- and Cam-dependent downstream effectors, may be instrumental for setting up the balance among axon degeneration, regeneration, and terminal differentiation.

In mammals, consideration of the role of NOS in neural injury and repair is confounded by the diverging functions of three NOS isoforms. Whereas the inducible NOS (iNOS) and the neuronal NOS (nNOS) contribute to Wallerian degeneration and thus promote axonal regrowth, the endothelial NOS (eNOS) interferes with and inhibits axon regrowth (Moreno-López, 2010). In *Drosophila*, there is only one Nos and our study supports its function as an inhibitor for axon regeneration *in vivo*. This is consistent with the recent report proposing NO as a switch during developmental remodeling of the *Drosophila* mushroom body axons: high level of NO promotes axon pruning while its reduction allows axon regrowth (Rabinovich et al., 2016).

Comprehensive studies to compare and contrast the machinery underlying axon and dendrite regeneration have only begun. Our previous work demonstrated a conserved growth program —the PTEN-Akt pathway, that regulates both dendrite and axon regeneration (Song et al., 2012). However, dendrite regeneration does not require the dual leucine kinase (DLK) injury-sensing pathway required for axon regeneration (Stone et al., 2014). Moreover, Piezo is differentially required in axons versus dendrites during neural repair, functioning as a specific inhibitor for axon regeneration. Thus, perhaps specific combinations of factors are required to fine-tune the microenvironment where neural injury takes place, and to effectively instruct axon or dendrite to mount an injury response and repair.

STAR★METHODS

CONTACT FOR REAGENT AND RESOURCE SHARING

Further information and requests for resources and reagents should be directed to and will be fulfilled by the Lead Contact, Yuh Nung Jan (yuhnung.jan@ucsf.edu).

EXPERIMENTAL MODEL AND SUBJECT DETAILS

Drosophila—*19–12-Gal4* (Xiang et al., 2010), *reop-Gal80* (Awasaki et al., 2008), *DmPiezoKO*, *UAS-DmPiezoRNAiv2796*, *DmPiezo-Gal4* (Kim et al., 2012), *ppk-CD4-tdGFP* (Han et al., 2011), *ppk-Gal4* (Han et al., 2011), *NompC-QF* (Petersen and Stowers, 2011), *QUAS-mCD8GFP* (Potter et al., 2010), *QUAS-mtdTomato* (Potter et al., 2010), *UAS-CD4TdTomato* (Han et al., 2011), *UAS-CamKII-I.Ala* (Joiner and Griffith, 1997), *UAS-CamKII RNAi* (Ashraf et al., 2006), *UAS-CamKII.T287D* (Jin et al., 1998), $Nos^{\Delta 15}$ (Yakubovich et al., 2010), Nos^{1}, *UAS-Nos* (Lacin et al., 2014), for^{k04703} (Spradling et al., 1999), $for^{11.247}$ (Eddison et al., 2012), *UAS-for-T1* (Belay et al., 2007), *UAS-dg2-P1*, *UAS-dg2-P2A* (MacPherson et al., 2004), *hsFLP;;UAS > CD2 > mCD8-GFP* (Grueber et al., 2007), *m12-Gal4* (*P(Gal4)tey*^{5053A}) (Ritzenthaler et al., 2000), *GCaMP6s* (Chen et al., 2013), Cam^{n339} (Heiman et al., 1996), *NompC-LexA* (Shearin et al., 2013) and $tub\text{-}Gal80^{ts}$ (McGuire et al., 2003) have been previously described. *UAS-Dcr-2*, $for^{DfED243}$, and *UAS-forRNAiBL35158* were from Bloomington stock center. *LexAop-myr-GCaMP6(s)* is a gift from the Freeman lab. To generate the *UAS-mPiezo1*, *UAS-hPiezo1*, *UAS-mPiezo1–2336-Myc* and *UAS-mPiezo1-TriM* stocks, the entire coding sequences were cloned into the PACU2 vector, and the constructs were then injected (Rainbow Transgenic Flies, Inc). Randomly selected male and female larvae were used. Analyses were not performed blind to the conditions of the experiments.

Mice—*Advillin-CreER* (Lau et al., 2011) mice were generously provided by S. Millar (University of Pennsylvania). $Piezo1^{fl/fl}$ (Cahalan et al., 2015) and *Rosa-stop-tdTomato* (Madisen et al., 2010) mice were obtained from Jackson Laboratories. All studies and procedures involving animal subjects were performed under the approval of the Institutional Animal Care and Use Committee (IACUC) at the University of Pennsylvania and Children's Hospital of Philadelphia. Four-week-old *Avil-CreER/Rosa-stop-tdTomato/*$Piezo1^{fl/+}$ and *Avil-CreER/Rosa-stop-tdTomato/*$Piezo1^{fl/fl}$ mice were administered 2 mg of tamoxifen daily by intraperitoneal injection for 5 consecutive days. 2-photon laser ablation was performed approximately 2 weeks after the last tamoxifen injection. Genomic DNA from the dorsal

root ganglia was extracted at the end of an experiment and then analyzed by PCR to confirm deletion. Age-matched mice with the same sex were randomly assigned to experimental groups. Analyses were not performed blind to the conditions of the experiments. All mice were housed in an animal facility and maintained in a temperature-controlled and light-controlled environment with an alternating 12-hour light/dark cycle. Up to 5 mice of the same sex and similar age were housed in a cage. The animals had no prior history of drug administration, surgery or behavioral testing.

Sensory axon lesion in Drosophila—Da neuron axon or dendrite lesion and imaging in the PNS or within the VNC were performed in live fly larvae as previously described (Song et al., 2012, 2015; Stone et al., 2014).

Drosophila motor nerve crush assay and quantification—As described previously (Xiong et al., 2010), the segmental nerves of 3rd instar larvae were pinched tightly through the cuticle for 5 s with Dumostar # 5 forceps, when the larvae were under CO_2 anesthesia. Larvae were then transferred to a grape plate and kept alive for varying periods of time at 25°C. For quantification of motor axon regeneration, the total volume of the growth cone at 2 and 14.5 hours after crush was measured.

METHOD DETAILS

Generation of clones for single axon analysis in flies—FLP-out clones were produced as previously described (Grueber et al., 2007).

Immunohistochemistry—Third instar larvae or cultured neurons were fixed according to standard protocols. The following antibodies were used: mouse anti-FasII 1D4 antiserum (1:2, Developmental Studies Hybridoma Bank), rabbit anti-Gap43 (1:1000, Novus Biologicals), mouse anti-MAP2 (1:1000, Sigma) rabbit anti-phospho-CaMKII alpha/beta/delta (Thr305) (1:50, Thermo Fisher Scientific), and fluorescence-conjugated secondary antibodies (1:1000, Jackson ImmunoResearch).

Generation of mutant construct—The triple mutant mPiezo1-TriM (E2133D + D2139E + D2144E) was generated using the QuickChange II XL site-directed mutagenesis kit according to the manufacturer's instructions, and confirmed by full-length DNA sequencing. The mutant was cloned into pcDNA3.1 (−) vector, which was modified to include an IRES-EGFP element.

Electrophysiological recordings and mechanical stimulation—As previously described (Yan et al., 2013), fillet preparations were made by dissecting 3rd instar larvae in haemolymph-like saline containing (in mM): 103 NaCl, 3 KCl, 5 TES, 10 trehalose, 10 glucose, 7 sucrose, 26 $NaHCO_3$, 1 NaH_2PO_4 and 4 $MgCl_2$, adjusted to pH 7.25 and 310 mOsm. 2 mM Ca^{2+} was added to the saline before use. Muscles covering the neurons were gently removed with forceps and to expose the da neurons. Action potentials were recorded extracellularly with a sample rate of 10 kHz and low-pass filtered at 2 kHz. A glass probe was driven by a piezo actuator mounted on a micromanipulator to give mechanical stimulation.

For whole-cell patch-clamp recordings, recording electrodes had a resistance of 2–3 MΩ when filled with internal solution composed of (in mM) 133 CsCl, 1 $CaCl_2$, 1 $MgCl_2$, 5 EGTA, 10 HEPES (pH 7.3 with CsOH), 4 MgATP and 0.4 Na_2GTP. The extracellular solution was composed of (in mM) 133 NaCl, 3 KCl, 2.5 $CaCl_2$, 1 $MgCl_2$, 10 HEPES (pH 7.3 with NaOH) and 10 glucose. For cell-attached patch-clamp recordings, external solution used to zero the membrane potential consisted of (in mM) 140 KCl, 1 $MgCl_2$, 10 glucose and 10 HEPES (pH 7.3 with KOH). Recording pipettes were of 2–3 MΩ resistance when filled with standard solution composed of (in mM) 130 mM NaCl, 5 KCl, 1 $CaCl_2$, 1 $MgCl_2$, 10 TEA-Cl and 10 HEPES (pH 7.3 with NaOH). Patch-clamp experiments were performed in standard whole-cell or cell-attached mode using Axopatch 200B amplifier (Axon Instruments). Currents were sampled at 20 kHz and filtered at 2 kHz. Leak currents before mechanical stimulations were subtracted offline from the current traces. For whole-cell recordings, mechanical stimulation was achieved using a fire-polished glass pipette (tip diameter 3–4 mm) positioned at an angle of 80° relative to the cell being recorded. Downward displacement of the probe toward the cell was driven by Clampex-controlled piezoelectric crystal microstage (E625 LVPZT Controller/Amplifier; Physik Instrumente). The probe had a velocity of 1 μm ms^{-1} during the ramp phase of the command for forward movement and the stimulus was applied for 150 ms. In the cell-attached patch clamp configuration, stretch activated currents were recorded by stimulating membrane patches with 500ms negative pressure pulses through the recording electrode using Clampex-controlled pressure clamp HSPC-1 device (ALA-scientific).

Quantitative analyses of sensory axon regeneration in flies—Quantification was performed as previously described (Song et al., 2012; Song et al., 2015). Briefly, for axon regeneration in the PNS, we used “Regeneration percentage,” which depicts the percent of regenerating axons among all the axons that were lesioned; “Regeneration length,” which measures the increase of axon length; “Regeneration index,” which is calculated as an increase of “axon length”/”distance between the cell body and the axon converging point (DCAC)” (Figure S1A). An axon is defined as regenerating only when it obviously regenerated beyond the retracted axon stem, and this was independently assessed of the other two parameters. “Regeneration index” is a better quantitative measurement of the extent of axon regeneration than “Regeneration length,” as it is normalized to the scaling of the larvae, which continue to grow in size during the course of the experiment. We still included the “Regeneration length” as a reference. For axon regeneration in the VNC, we used “Regeneration percentage,” which depicts the percent of regenerating commissure segments among all the segments that were severed; “Terminal branching,” which counts the number of axons that regenerated, reached the commissure bundle and appeared to form elaborate branches; “Commissure regrowth,” which counts the number of axons that had regenerated to connect the boundaries of commissure segments, longitudinally or laterally. The regeneration parameters from various genotypes were compared to that of the WT if not noted otherwise, and only those with significant difference were labeled with the asterisks.

Live imaging in flies—Live imaging was performed as described (Emoto et al., 2006; Parrish et al., 2007). Embryos were collected for 2 hours on yeasted grape juice agar plates and were aged at 25°C or room temperature. At the appropriate time, a single lava was

mounted in 90% glycerol under coverslips sealed with grease, imaged using a Leica SP5 or Zeiss LSM 880 microscope, and returned to grape juice agar plates between imaging sessions.

GCaMP imaging and analysis in flies—Calcium imaging was performed using the membrane targeting myr-GCaMP6(s) in 3rd instar larvae *in vivo*. Larvae were immobilized with ether anesthesia. Each axotomized class III da neuron was imaged by a Z stack with 0.2 Hz frame frequency for 500 s (5 s duration per frame for 100 frames). The GCaMP fluorescence signal in each frame was subtracted and divided by the average fluorescence intensity of ROI in the 100 frames for each neuron, to normalize the baseline to 0. The fast Fourier transform (FFT) algorithm in MATLAB was then applied to decompose the fluorescence function of time into frequency components. The frequency domain representation of the original signal is shown by magnitude spectrum. The y axis indicates the relative amplitude of fluorescence vibration after FFT at the specific frequency of the x axis.

Quantitative RT-PCR—Semiquantitative RT-PCR was done for *for* and a*-tubulin* according to the manufacturer's protocols. The sequences were as follows: three regions of the *for* transcripts were amplified with primers *for F1* 5′-gtcgggtcagaatttccaga-3′, *for F2* 5′-cagaggattcccaggatcaa-3′, *for F3* 5′-ggaaaagtgcgagtgacgat-3′ and *for R* 5′-agtttggaccagctctacgc-3′. a*-tubulin* was amplified with 5′-acaacgaggctatctacgaca-3′ and 5′-ttttcagtgttgcagtgaattt-3′.

Microfluidic neuron culture and axotomy—For axotomy and staining, house-made microfluidic devices were used.

Chip design and master production: The microfluidic device was made up of two elements: macro-chambers (length 7000 um, width 1200 um, height 250 um) for cell or fluid injection, separated by narrowing arrays micro-channels (length 450 um, width 10 um, height 3 um) allowing directional axonal outgrowth. To produce the template with elements of two different thicknesses, two layers of photoresist (SU8 5 and SU8 2150) were used. First layer of SU8 5 (Microchem, USA) was spin-coated onto the wafer at 500 rpm for 5 s and 3000 rpm for 60 s. It was soft baked at 65°C for 2 min and 96°C for 5 min. The template was then exposed to UV light through a house-made high-resolution transparency chrome mask for 30 s at 365 nm and 275 W. The wafer was hard baked at 65°C for 1 min and 95°C for 2 min. After the hard bake, the channels (3 um high) were developed in SU8 developer for 2 min and rinsed with isopropyl alcohol and dried with pressurized nitrogen gas. The injection channels were then produced by laminating the newly obtained wafer with a 250 mm thick of SU8 2150. The second layer of SU8 2150 (Microchem,USA) was spin-coated onto the wafer at 500 rpm for 10 s and 2250 rpm for 60 s. It was soft baked at 65°C for 7 min and 95°C for 60 min. The template was then exposed to UV light for 120 s at 365 nm and 275 W. The wafer was hard baked at 65°C for 5 min and 95°C for 20 min. After the hard bake, the channels (250 um high) were developed in SU8 developer overnight and rinsed with isopropyl alcohol and dried with pressurized nitrogen gas.

Microfluidic chip production: Polydimethylsiloxane (PDMS, Sylgard 184, Dow Corning, USA) was mixed thoroughly with a curing agent (9:1 ratio). The resulting preparation was poured onto the master and degassed in a vacuum desiccator for 3 h. The polyester resin replicate was cured at 80°C for 6 h. The elastomeric polymer print was detached and reservoirs were punched for each macro-channel.

Microfluidics culture platform fabrication: The PDMS pieces were sterilized with 70% ethanol and exposed to UV (254 nm) for 10 min. All following work performed with microfluidics devices was done aseptically in a biosafety cabinet. Once dried, the PDMS pieces were gently pressed on the cover glass (Fisher Scientific Premium Cover Glass sized: 24×60–1 mm) until a complete seal formed and no bubbles remained between the PDMS molds and glass surface. The cover glass had been previously coated in 0.1 mg/ml poly-D-lysine for 48 h, washed 5 times in sterile double distilled water, and thoroughly dried via aspiration.

Neuronal culture for microfluidic device and treatments: hippocampal neurons were dissociated from embryonic rat (E18) by the Neurons R Us Culture Service Center at the University of Pennsylvania. Approximately 1×10^5 cells were seeded on the soma side of the chamber. A total of 600 ml standard neuron medium was added to the wells of the soma side to establish a 100 μl volume difference between somal and axonal compartments and to maintain fluidically isolated microenvironment on the axonal side. Fresh complete medium was added to each PDMS pieces every three days. On DIV7, axotomy was achieved by rapid aspiration and quick washes with double distilled water and standard neuron media on the axon side. 30 mM of Yoda1 or DMSO vehicle control was added to the axonal chamber for 24 h and a volume difference of 100 μl between the two compartments was again maintained. Axon regeneration was assessed after fixation and by immunocytochemistry.

For quantitative analysis of axon growth before and after axotomy, axons in the terminal chamber labeled by Gap43 staining were imaged using a Leica TCS SP8 laser scanning microscope with a 40 × objective. Axon coverage area was calculated by connecting the tips of the distal axons. Axon coverage area was normalized to the Normalization length to obtain the Normalized regeneration (Figure S8B). Images were collected from multiple chambers in at least 6 experiments.

In vivo imaging in mice—For intravital imaging of the mouse corneal nerves a customized stage was used to immobilize the head of anesthetized mice and expose the eye globe, including the entire cornea. Mice were anaesthetized with intraperitoneal injection of ketamine and xylazine (15 mg ml^{-1} and 1 mg ml^{-1}, respectively in PBS). Mice were then placed under the microscope onto a heating pad and kept anesthetized with a continuous delivery of isoflurane through a nose cone (1% in air). Image acquisition of the live cornea was performed with an Olympus FV1200MPE microscope, equipped with a Chameleon Vision II Ti:Sapphire laser. A laser beam was focused through a 10X or 20X objective lens (Olympus UPLSAPO10X2, N.A. 0.40; UPLSAPO20X, N.A. 0.75) and used to scan a $1mm^2$ or 0.5 mm^2 field of view, respectively. Serial optical sections were acquired in 3–4 mm steps, starting from the surface of the eye and capturing the entire thickness of the cornea

(epithelium ~40 μm, stroma ~80 μm). For each time point, inherent landmarks within the cornea were used to consistently navigate back to the original regions.

Laser ablation of corneal sensory nerves and quantification of corneal sensory nerve regeneration—*In vivo* laser axotomy was performed using the same 2-photon laser used for imaging. The laser beam was focused on the deeper layers of the corneal stroma where the larger nerve trunks are located before they branch into thinner fibers that form the subbasal nerve plexus. The laser was guided to scan a small (10×10 μm) area at specific branch points of the corneal nerves within the stroma, using the following settings: 850 nm wavelength, 100% laser power, 1 s exposure. Immediately after ablation, the microscope was switched to imaging mode and a series of serial optical sections were collected to visualize and validate that the laser ablation was effective. Serial optical sections of the entire cornea were collected immediately before and 24 h after laser ablation of the corneal nerves to validate the degeneration of nerve fibers downstream of the sites of ablation.

To quantify sensory nerve regeneration, a region of interest (ROI) was defined by outlining the border between the nerve endings and the vacant space. All the axons within the ROI were manually traced and measured, and the total axon length was calculated for D2, 4 and 7 post-ablation. The regrown axon length was calculated as the increase between D4 and D2 (Δ2 Days), or between D7 and D2 (Δ5 Days). This value was normalized to Normalization length A (the length of the curvature in-between the two nerve ending boarders with a radius of 556.5 μm) or Normalization length B (the length of the interface between the nerve endings and the vacant space), to obtain Normalization regeneration A or B, respectively (Figure S8D).

QUANTIFICATION AND STATISTICAL ANALYSIS

No statistical methods were used to pre-determine sample sizes but our sample sizes are similar to those reported in previous publications (Song et al., 2012; Song et al., 2015), and the statistical analyses were done afterward without interim data analysis. Data distribution was assumed to be normal but this was not formally tested. All data were collected and processed randomly. Each experiment was successfully reproduced at least three times and was performed on different days. The values of “N” (sample size) are provided in the figure legends. Data are expressed as mean ± SEM in bar graphs. No data points were excluded. Two-tailed unpaired Student’s t test was performed for comparison between two groups of samples. One-way ANOVA followed by multiple comparison test was performed for comparisons among three or more groups of samples. Two-way ANOVA followed by multiple comparison test was performed for comparisons between two or more curves. Fisher’s exact test was used to compare the percentage. Statistical significance was assigned, *$p < 0.05$, **$p < 0.01$, ***$p < 0.001$.

Supplementary Material

Refer to Web version on PubMed Central for supplementary material.

ACKNOWLEDGMENTS

We thank S. Younger, J. Mathur, T. Cheng, W. Zhang, and J. Goldshteyn for technical assistance; P.H. O'Farrell for advice on the Nos pathway and comments for the manuscript; S. Kune, M. Eddison, M. Sokolowski, S. Davies, Y. Guo, M. Freeman, Z. Ma, and A. Sheehan for fly lines; Bloomington Stock Centre and VDRC for fly stocks; J. Wood for plasmids; the Neurons R Us Culture Service Center of PTNC at the University of Pennsylvania for providing cultured neurons; the Krishna P. Singh Center for Nanotechnology at the University of Pennsylvania for supporting the microfluidic device; members of the Jan lab and Song lab for helpful discussions. Y.S. is a recipient of the National Institute of Neurological Disorders and Stroke (NINDS) Pathway to Independence Award. This work was supported by an IDDRC New Program Development Award (CHOP/Penn), an NINDS K99/R00 award (5K99NS088211–02 and R00NS088211), and an NIH grant (1R01NS107392–01) to Y.S., and NIH grants (2R37NS040929 and R35NS097227) to Y.N.J. A.P., L.Y.J. Y.N.J. are investigators of Howard Hughes Medical Institute.

REFERENCES

Albuisson J, Murthy SE, Bandell M, Coste B, Louis-Dit-Picard H, Mathur J, Fénéant-Thibault M, Tertian G, de Jaureguiberry JP, Syfuss PY, et al. (2013). Dehydrated hereditary stomatocytosis linked to gain-of-function mutations in mechanically activated PIEZO1 ion channels. Nat. Commun 4, 1884. [PubMed: 23695678]

Andolfo I, Alper SL, De Franceschi L, Auriemma C, Russo R, De Falco L, Vallefuoco F, Esposito MR, Vandorpe DH, Shmukler BE, et al. (2013). Multiple clinical forms of dehydrated hereditary stomatocytosis arise from mutations in PIEZO1. Blood 121, 3925–3935. [PubMed: 23479567]

Ashraf SI, McLoon AL, Sclarsic SM, and Kunes S (2006). Synaptic protein synthesis associated with memory is regulated by the RISC pathway in Drosophila. Cell 124, 191–205. [PubMed: 16413491]

Awasaki T, Lai SL, Ito K, and Lee T (2008). Organization and postembryonic development of glial cells in the adult central brain of Drosophila. J. Neurosci 28, 13742–13753. [PubMed: 19091965]

Bae C, Gnanasambandam R, Nicolai C, Sachs F, and Gottlieb PA (2013). Xerocytosis is caused by mutations that alter the kinetics of the mechanosensitive channel PIEZO1. Proc. Natl. Acad. Sci. USA 110, E1162–E1168. [PubMed: 23487776]

Belay AT, Scheiner R, So AK, Douglas SJ, Chakaborty-Chatterjee M, Levine JD, and Sokolowski MB (2007). The foraging gene of Drosophila melanogaster: Spatial-expression analysis and sucrose responsiveness. J. Comp. Neurol 504, 570–582. [PubMed: 17701979]

Beneteau C, Thierry G, Blesson S, Le Vaillant C, Picard V, Béné MC, Eveillard M, and Le Caignec C (2014). Recurrent mutation in the PIEZO1 gene in two families of hereditary xerocytosis with fetal hydrops. Clin. Genet 85, 293–295. [PubMed: 23581886]

Blumenthal NR, Hermanson O, Heimrich B, and Shastri VP (2014). Stochastic nanoroughness modulates neuron-astrocyte interactions and function via mechanosensing cation channels. Proc. Natl. Acad. Sci. USA 111, 16124–16129. [PubMed: 25349433]

Bray D (1984). Axonal growth in response to experimentally applied mechanical tension. Dev. Biol 102, 379–389. [PubMed: 6706005]

Cahalan SM, Lukacs V, Ranade SS, Chien S, Bandell M, and Patapoutian A (2015). Piezo1 links mechanical forces to red blood cell volume. eLife 4 Published online May 22, 2015. 10.7554/eLife.07370.

Chalfie M (2009). Neurosensory mechanotransduction. Nat. Rev. Mol. Cell Biol 10, 44–52. [PubMed: 19197331]

Chen TW, Wardill TJ, Sun Y, Pulver SR, Renninger SL, Baohan A, Schreiter ER, Kerr RA, Orger MB, Jayaraman V, et al. (2013). Ultrasensitive fluorescent proteins for imaging neuronal activity. Nature 499, 295–300. [PubMed: 23868258]

Chen X, Wanggou S, Bodalia A, Zhu M, Dong W, Fan JJ, Yin WC, Min HK, Hu M, Draghici D, et al. (2018). A feedforward mechanism mediated by mechanosensitive ion channel PIEZO1 and tissue mechanics promotes glioma aggression. Neuron 100, 799–815. [PubMed: 30344046]

Coste B, Mathur J, Schmidt M, Earley TJ, Ranade S, Petrus MJ, Dubin AE, and Patapoutian A (2010). Piezo1 and Piezo2 are essential components of distinct mechanically activated cation channels. Science 330, 55–60. [PubMed: 20813920]

Coste B, Xiao B, Santos JS, Syeda R, Grandl J, Spencer KS, Kim SE, Schmidt M, Mathur J, Dubin AE, et al. (2012). Piezo proteins are pore-forming subunits of mechanically activated channels. Nature 483, 176–181. [PubMed: 22343900]

Coste B, Houge G, Murray MF, Stitziel N, Bandell M, Giovanni MA, Philippakis A, Hoischen A, Riemer G, Steen U, et al. (2013). Gain-of-function mutations in the mechanically activated ion channel PIEZO2 cause a sub-type of Distal Arthrogryposis. Proc. Natl. Acad. Sci. USA 110, 4667–4672. [PubMed: 23487782]

Coste B, Murthy SE, Mathur J, Schmidt M, Mechioukhi Y, Delmas P, and Patapoutian A (2015). Piezo1 ion channel pore properties are dictated by C-terminal region. Nat. Commun 6, 7223. [PubMed: 26008989]

Davies SA (2006). Signalling via cGMP: Lessons from Drosophila. Cell. Signal 18, 409–421. [PubMed: 16260119]

Eddison M, Belay AT, Sokolowski MB, and Heberlein U (2012). A genetic screen for olfactory habituation mutations in Drosophila: analysis of novel foraging alleles and an underlying neural circuit. PLoS ONE 7, e51684. [PubMed: 23284741]

Emoto K, Parrish JZ, Jan LY, and Jan YN (2006). The tumour suppressor Hippo acts with the NDR kinases in dendritic tiling and maintenance. Nature 443, 210–213. [PubMed: 16906135]

Enes J, Langwieser N, Ruschel J, Carballosa-Gonzalez MM, Klug A, Traut MH, Ylera B, Tahirovic S, Hofmann F, Stein V, et al. (2010). Electrical activity suppresses axon growth through Ca(v)1.2 channels in adult primary sensory neurons. Curr. Biol 20, 1154–1164. [PubMed: 20579880]

Faucherre A, Kissa K, Nargeot J, Mangoni ME, and Jopling C (2014). Piezo1 plays a role in erythrocyte volume homeostasis. Haematologica 99, 70–75.

Franze K, Janmey PA, and Guck J (2013). Mechanics in neuronal development and repair. Annu. Rev. Biomed. Eng 15, 227–251. [PubMed: 23642242]

Gottlieb PA, Barone T, Sachs F, and Plunkett R (2010). Neurite outgrowth from PC12 cells is enhanced by an inhibitor of mechanical channels. Neurosci. Lett 481, 115–119. [PubMed: 20600595]

Griffith LC (2004). Regulation of calcium/calmodulin-dependent protein kinase II activation by intramolecular and intermolecular interactions. J. Neurosci 24, 8394–8398. [PubMed: 15456810]

Grueber WB, Ye B, Yang CH, Younger S, Borden K, Jan LY, and Jan YN (2007). Projections of Drosophila multidendritic neurons in the central nervous system: Links with peripheral dendrite morphology. Development 134, 55–64. [PubMed: 17164414]

Han C, Jan LY, and Jan YN (2011). Enhancer-driven membrane markers for analysis of nonautonomous mechanisms reveal neuron-glia interactions in Drosophila. Proc. Natl. Acad. Sci. USA 108, 9673–9678. [PubMed: 21606367]

Heiman RG, Atkinson RC, Andruss BF, Bolduc C, Kovalick GE, and Beckingham K (1996). Spontaneous avoidance behavior in Drosophila null for calmodulin expression. Proc. Natl. Acad. Sci. USA 93, 2420–2425. [PubMed: 8637889]

Huang S, and Rompolas P (2017). Two-photon microscopy for intracutaneous imaging of stem cell activity in mice. Exp. Dermatol 26, 379–383. [PubMed: 27676122]

Hung WC, Yang JR, Yankaskas CL, Wong BS, Wu PH, Pardo-Pastor C, Serra SA, Chiang MJ, Gu Z, Wirtz D, et al. (2016). Confinement sensing and signal optimization via Piezo1/PKA and Myosin II pathways. Cell Rep. 15, 1430–1441. [PubMed: 27160899]

Jaalouk DE, and Lammerding J (2009). Mechanotransduction gone awry. Nat. Rev. Mol. Cell Biol 10, 63–73. [PubMed: 19197333]

Jacques-Fricke BT, Seow Y, Gottlieb PA, Sachs F, and Gomez TM (2006). Ca2+ influx through mechanosensitive channels inhibits neurite outgrowth in opposition to other influx pathways and release from intracellular stores. J. Neurosci 26, 5656–5664. [PubMed: 16723522]

Jin P, Griffith LC, and Murphey RK (1998). Presynaptic calcium/calmodulin-dependent protein kinase II regulates habituation of a simple reflex in adult Drosophila. J. Neurosci 18, 8955–8964. [PubMed: 9787001]

Joiner M.l.A., and Griffith LC (1997). CaM kinase II and visual input modulate memory formation in the neuronal circuit controlling courtship conditioning. J. Neurosci 17, 9384–9391. [PubMed: 9364084]

Kerstein PC, Jacques-Fricke BT, Rengifo J, Mogen BJ, Williams JC, Gottlieb PA, Sachs F, and Gomez TM (2013). Mechanosensitive TRPC1 channels promote calpain proteolysis of talin to regulate spinal axon outgrowth. J. Neurosci 33, 273–285. [PubMed: 23283340]

Kim SE, Coste B, Chadha A, Cook B, and Patapoutian A (2012). The role of Drosophila Piezo in mechanical nociception. Nature 483, 209–212. [PubMed: 22343891]

Koser DE, Thompson AJ, Foster SK, Dwivedy A, Pillai EK, Sheridan GK, Svoboda H, Viana M, Costa LD, Guck J, et al. (2016). Mechanosensing is critical for axon growth in the developing brain. Nat. Neurosci 19, 1592–1598. [PubMed: 27643431]

Lacin H, Rusch J, Yeh RT, Fujioka M, Wilson BA, Zhu Y, Robie AA, Mistry H, Wang T, Jaynes JB, and Skeath JB (2014). Genome-wide identification of Drosophila Hb9 targets reveals a pivotal role in directing the transcriptome within eight neuronal lineages, including activation of nitric oxide synthase and Fd59a/Fox-D. Dev. Biol 388, 117–133. [PubMed: 24512689]

Lamoureux P, Buxbaum RE, and Heidemann SR (1989). Direct evidence that growth cones pull. Nature 340, 159–162. [PubMed: 2739738]

Lau J, Minett MS, Zhao J, Dennehy U, Wang F, Wood JN, and Bogdanov YD (2011). Temporal control of gene deletion in sensory ganglia using a tamoxifen-inducible Advillin-Cre-ERT2 recombinase mouse. Mol. Pain 7, 100. [PubMed: 22188729]

Li J, Hou B, Tumova S, Muraki K, Bruns A, Ludlow MJ, Sedo A, Hyman AJ, McKeown L, Young RS, et al. (2014). Piezo1 integration of vascular architecture with physiological force. Nature 515, 279–282. [PubMed: 25119035]

MacPherson MR, Lohmann SM, and Davies SA (2004). Analysis of Drosophila cGMP-dependent protein kinases and assessment of their in vivo roles by targeted expression in a renal transporting epithelium. J. Biol. Chem 279, 40026–40034. [PubMed: 15218025]

Madisen L, Zwingman TA, Sunkin SM, Oh SW, Zariwala HA, Gu H, Ng LL, Palmiter RD, Hawrylycz MJ, Jones AR, et al. (2010). A robust and high-throughput Cre reporting and characterization system for the whole mouse brain. Nat. Neurosci 13, 133–140. [PubMed: 20023653]

Maksimovic S, Nakatani M, Baba Y, Nelson AM, Marshall KL, Wellnitz SA, Firozi P, Woo SH, Ranade S, Patapoutian A, and Lumpkin EA (2014). Epidermal Merkel cells are mechanosensory cells that tune mammalian touch receptors. Nature 509, 617–621. [PubMed: 24717432]

Marletta MA (1994). Nitric oxide synthase: Aspects concerning structure and catalysis. Cell 78, 927–930. [PubMed: 7522970]

McGuire SE, Le PT, Osborn AJ, Matsumoto K, and Davis RL (2003). Spatiotemporal rescue of memory dysfunction in Drosophila. Science 302, 1765–1768. [PubMed: 14657498]

McMillin MJ, Beck AE, Chong JX, Shively KM, Buckingham KJ, Gildersleeve HI, Aracena MI, Aylsworth AS, Bitoun P, Carey JC, et al.; University of Washington Center for Mendelian Genomics (2014). Mutations in PIEZO2 cause Gordon syndrome, Marden-Walker syndrome, and distal arthrogryposis type 5. Am. J. Hum. Genet 94, 734–744. [PubMed: 24726473]

Moreno-López B (2010). Local isoform-specific NOS inhibition: A promising approach to promote motor function recovery after nerve injury. J. Neurosci. Res 88, 1846–1857. [PubMed: 20143424]

Müller LJ, Pels L, and Vrensen GF (1996). Ultrastructural organization of human corneal nerves. Invest. Ophthalmol. Vis. Sci 37, 476–488. [PubMed: 8595948]

Müller LJ, Marfurt CF, Kruse F, and Tervo TM (2003). Corneal nerves: Structure, contents and function. Exp. Eye Res 76, 521–542. [PubMed: 12697417]

Nathan C, and Xie QW (1994). Nitric oxide synthases: Roles, tolls, and controls. Cell 78, 915–918. [PubMed: 7522969]

Nilius B, and Honoré E (2012). Sensing pressure with ion channels. Trends Neurosci. 35, 477–486. [PubMed: 22622029]

Park D, Coleman MJ, Hodge JJ, Budnik V, and Griffith LC (2002). Regulation of neuronal excitability in Drosophila by constitutively active CaMKII. J. Neurobiol 52, 24–42. [PubMed: 12115891]

Parrish JZ, Emoto K, Kim MD, and Jan YN (2007). Mechanisms that regulate establishment, maintenance, and remodeling of dendritic fields. Annu. Rev. Neurosci 30, 399–423. [PubMed: 17378766]

Pathak MM, Nourse JL, Tran T, Hwe J, Arulmoli J, Le DT, Bernardis E, Flanagan LA, and Tombola F (2014). Stretch-activated ion channel Piezo1 directs lineage choice in human neural stem cells. Proc. Natl. Acad. Sci. USA 111, 16148–16153. [PubMed: 25349416]

Petersen LK, and Stowers RS (2011). A Gateway MultiSite recombination cloning toolkit. PLoS ONE 6, e24531. [PubMed: 21931740]

Pfister BJ, Iwata A, Meaney DF, and Smith DH (2004). Extreme stretch growth of integrated axons. J. Neurosci 24, 7978–7983. [PubMed: 15356212]

Pfister BJ, Bonislawski DP, Smith DH, and Cohen AS (2006). Stretch-grown axons retain the ability to transmit active electrical signals. FEBS Lett. 580, 3525–3531. [PubMed: 16730003]

Potter CJ, Tasic B, Russler EV, Liang L, and Luo L (2010). The Q system: a repressible binary system for transgene expression, lineage tracing, and mosaic analysis. Cell 141, 536–548. [PubMed: 20434990]

Rabinovich D, Yaniv SP, Alyagor I, and Schuldiner O (2016). Nitric oxide as a switching mechanism between axon degeneration and regrowth during developmental remodeling. Cell 164, 170–182. [PubMed: 26771490]

Ranade SS, Qiu Z, Woo SH, Hur SS, Murthy SE, Cahalan SM, Xu J, Mathur J, Bandell M, Coste B, et al. (2014a). Piezo1, a mechanically activated ion channel, is required for vascular development in mice. Proc. Natl. Acad. Sci. USA 111, 10347–10352. [PubMed: 24958852]

Ranade SS, Woo SH, Dubin AE, Moshourab RA, Wetzel C, Petrus M, Mathur J, Bégay V, Coste B, Mainquist J, et al. (2014b). Piezo2 is the major transducer of mechanical forces for touch sensation in mice. Nature 516, 121–125. [PubMed: 25471886]

Regulski M, and Tully T (1995). Molecular and biochemical characterization of dNOS: a Drosophila Ca2+/calmodulin-dependent nitric oxide synthase. Proc. Natl. Acad. Sci. USA 92, 9072–9076. [PubMed: 7568075]

Ritzenthaler S, Suzuki E, and Chiba A (2000). Postsynaptic filopodia in muscle cells interact with innervating motoneuron axons. Nat. Neurosci 3, 1012–1017. [PubMed: 11017174]

Rompolas P, Deschene ER, Zito G, Gonzalez DG, Saotome I, Haberman AM, and Greco V (2012). Live imaging of stem cell and progeny behaviour in physiological hair-follicle regeneration. Nature 487, 496–499. [PubMed: 22763436]

Schimmelpfennig B (1982). Nerve structures in human central corneal epithelium. Graefes Arch. Clin. Exp. Ophthalmol 218, 14–20. [PubMed: 7056476]

Shearin HK, Dvarishkis AR, Kozeluh CD, and Stowers RS (2013). Expansion of the gateway multisite recombination cloning toolkit. PLoS ONE 8, e77724. [PubMed: 24204935]

Shmukler BE, Vandorpe DH, Rivera A, Auerbach M, Brugnara C, and Alper SL (2014). Dehydrated stomatocytic anemia due to the heterozygous mutation R2456H in the mechanosensitive cation channel PIEZO1: A case report. Blood Cells Mol. Dis 52, 53–54. [PubMed: 23973043]

Smith DH (2009). Stretch growth of integrated axon tracts: extremes and exploitations. Prog. Neurobiol 89, 231–239. [PubMed: 19664679]

Song Y, Ori-McKenney KM, Zheng Y, Han C, Jan LY, and Jan YN (2012). Regeneration of Drosophila sensory neuron axons and dendrites is regulated by the Akt pathway involving Pten and microRNA bantam. Genes Dev. 26, 1612–1625. [PubMed: 22759636]

Song Y, Sretavan D, Salegio EA, Berg J, Huang X, Cheng T, Xiong X, Meltzer S, Han C, Nguyen TT, et al. (2015). Regulation of axon regeneration by the RNA repair and splicing pathway. Nat. Neurosci 18, 817–825. [PubMed: 25961792]

Spradling AC, Stern D, Beaton A, Rhem EJ, Laverty T, Mozden N, Misra S, and Rubin GM (1999). The Berkeley Drosophila Genome Project gene disruption project: Single P-element insertions mutating 25% of vital Drosophila genes. Genetics 153, 135–177. [PubMed: 10471706]

Stone MC, Albertson RM, Chen L, and Rolls MM (2014). Dendrite injury triggers DLK-independent regeneration. Cell Rep. 6, 247–253. [PubMed: 24412365]

Suter DM, and Miller KE (2011). The emerging role of forces in axonal elongation. Prog. Neurobiol 94, 91–101. [PubMed: 21527310]

Syeda R, Xu J, Dubin AE, Coste B, Mathur J, Huynh T, Matzen J, Lao J, Tully DC, Engels IH, et al. (2015). Chemical activation of the mechanotransduction channel Piezo1. eLife 4 Published online May 22, 2015 10.7554/eLife.07369.

Tedeschi A, Dupraz S, Laskowski CJ, Xue J, Ulas T, Beyer M, Schultze JL, and Bradke F (2016). The calcium channel subunit Alpha2delta2 suppresses axon regeneration in the adult CNS. Neuron 92, 419–434. [PubMed: 27720483]

Woo SH, Ranade S, Weyer AD, Dubin AE, Baba Y, Qiu Z, Petrus M, Miyamoto T, Reddy K, Lumpkin EA, et al. (2014). Piezo2 is required for Merkel-cell mechanotransduction. Nature 509, 622–626. [PubMed: 24717433]

Woo SH, Lukacs V, de Nooij JC, Zaytseva D, Criddle CR, Francisco A, Jessell TM, Wilkinson KA, and Patapoutian A (2015). Piezo2 is the principal mechanotransduction channel for proprioception. Nat. Neurosci 18, 1756–1762. [PubMed: 26551544]

Wu J, Lewis AH, and Grandl J (2017). Touch, tension, and transduction—The function and regulation of piezo ion channels. Trends Biochem. Sci 42, 57–71. [PubMed: 27743844]

Xiang Y, Yuan Q, Vogt N, Looger LL, Jan LY, and Jan YN (2010). Light-avoidance-mediating photoreceptors tile the Drosophila larval body wall. Nature 468, 921–926. [PubMed: 21068723]

Xiong X, Wang X, Ewanek R, Bhat P, Diantonio A, and Collins CA (2010). Protein turnover of the Wallenda/DLK kinase regulates a retrograde response to axonal injury. J. Cell Biol 191, 211–223. [PubMed: 20921142]

Yakubovich N, Silva EA, and O'Farrell PH (2010). Nitric oxide synthase is not essential for Drosophila development. Curr. Biol 20, R141–R142. [PubMed: 20178753]

Yan Z, Zhang W, He Y, Gorczyca D, Xiang Y, Cheng LE, Meltzer S, Jan LY, and Jan YN (2013). Drosophila NOMPC is a mechanotransduction channel subunit for gentle-touch sensation. Nature 493, 221–225. [PubMed: 23222543]

Zarychanski R, Schulz VP, Houston BL, Maksimova Y, Houston DS, Smith B, Rinehart J, and Gallagher PG (2012). Mutations in the mechanotransduction protein PIEZO1 are associated with hereditary xerocytosis. Blood 120, 1908–1915. [PubMed: 22529292]

Zhou B, Yu P, Lin MY, Sun T, Chen Y, and Sheng ZH (2016). Facilitation of axon regeneration by enhancing mitochondrial transport and rescuing energy deficits. J. Cell Biol 214, 103–119. [PubMed: 27268498]

Highlights

- Piezo cell autonomously inhibits axon regeneration in *Drosophila* sensory neurons
- Piezo channels are activated after axon injury or during axon regeneration
- Piezo inhibits axon regeneration through calcium signaling, Nos, and PKG
- Piezo1 also inhibits axon regeneration in mammals *in vitro* and *in vivo*

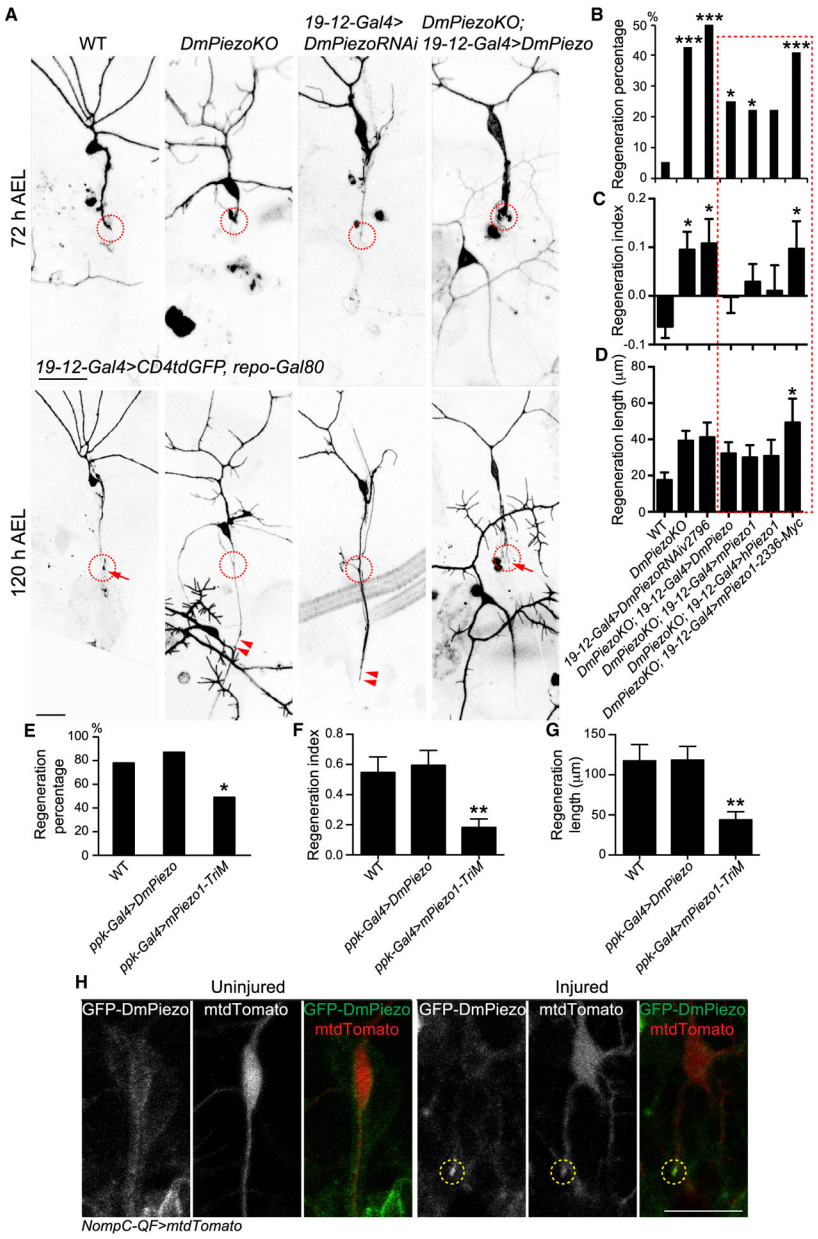

Figure 1. *DmPiezo* Inhibits Axon Regeneration in da Sensory Neurons

(A) Class III da neuron axons fail to regenerate in WT. *DmPiezo* removal as in *DmPiezoKO* and class III da neuron-specific RNAi leads to increased axon regeneration. Class III da neuron-specific expression of *DmPiezo* suppressed the enhanced regeneration in *DmPiezoKO*. The injury site is demarcated by the dashed circle. Arrow marks axon stalling, while arrowheads show the regrowing axon tips.

(B–D) Quantification of class III da neuron axon regeneration with regeneration percentage (B), regeneration index (C), and regeneration length (D). Class III da neuron expression of DmPiezo, mPiezo1, or hPiezo1, but not mPiezo1–2336-Myc rescues the regeneration phenotype in *DmPiezoKO*. n = 22–49 neurons from 6 to 16 larvae.

(E–G) Quantification of class IV da neuron axon regeneration with regeneration percentage (E), regeneration index (F), and regeneration length (G). Over-expression of the over-activating mPiezo1-TriM reduces class IV da neuron axon regeneration. n = 15–29 neurons from 4 to 7 larvae.

(H) GFP-DmPiezo is present diffusely in the cell body and axon of uninjured class III da neurons. 24 hr AI, GFP-DmPiezo is enriched in the tip of the growth cone (dashed circle). Data are expressed as mean ± SEM in bar graphs in all figures. *p < 0.05, **p < 0.01, ***p < 0.001 by Fisher's exact test (B and E), one-way ANOVA followed by Holm-Sidak's test (C) or Dunnett's test (D, F, and G). Scale bar, 20 μm.

See also Figure S1.

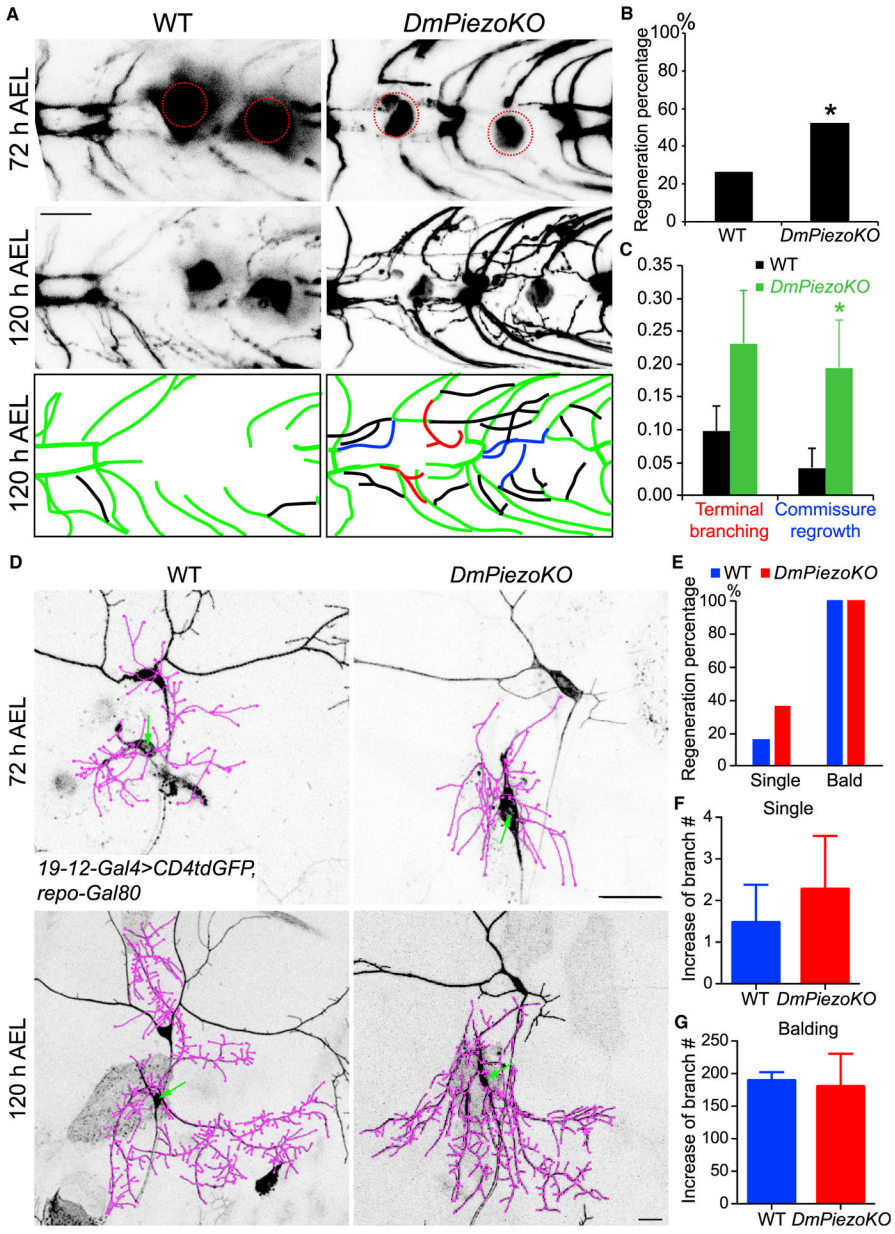

Figure 2. Removal of *DmPiezo* Enhances Axon Regeneration in the CNS but Does Not Improve Dendrite Regeneration

(A) *DmPiezo* removal increases class IV da neuron axon regrowth in the VNC. The injury site is demarcated by the dashed circle. The regenerating axons are illustrated in schematic diagrams with terminal branching marked in red, commissure regrowth in blue, and other regrowing axons in black.

(B) Compared to WT, which shows limited regrowth, the regeneration percentage is increased in *DmPiezoKO*. n = 29–52 injured segments from 13 to 32 larvae.

(C) *DmPiezoKO* increases terminal branching and commissure regrowth of class IV da neurons after injury in the VNC. n = 13–32 larvae.

(D) Both WT and *DmPiezoKO* regrow dendrites after balding. The new dendrites are traced and marked in pink. The soma of the balded neuron is marked by arrows.
(E) Regeneration percentage is similar between WT and *DmPiezoKO*.
(F and G) There is no difference in the increase of dendritic branches between WT and *DmPiezoKO*, after single dendrite lesion (F) or balding (G). n = 11–18 neurons from 4 to 8 larvae for single-dendrite injury, and 3–6 neurons from 2 to 5 larvae for balding.
*$p < 0.05$ by Fisher's exact test (B and E) and two-tailed unpaired Student's t test (C, F, and G). Scale bar, 20 μm.
See also Figure S2.

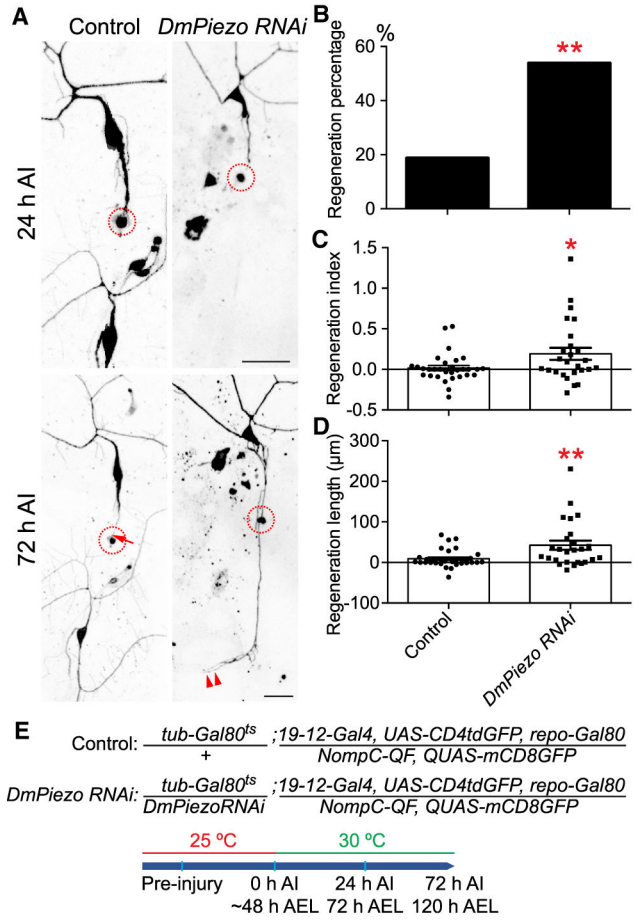

Figure 3. Knocking Down DmPiezo Specifically after Injury Is Sufficient to Promote Axon Regeneration

(A) DmPiezo is knocked down in class III da neurons with DmPiezo RNAi using the temperature-sensitive Gal80^{ts}, which is expressed in all cells by the *tubulin* (*tub*) promoter. Larvae were raised at the permissive temperature at 25°C until injury and then kept at the restrictive temperature at 30°C to allow DmPiezo RNAi expression. Knockdown DmPiezo specifically after injury is sufficient to promote axon regeneration. The injury site is demarcated by the dashed circle. Arrow marks axon stalling while arrowheads show the regrowing axon tips.

(B–D) Quantification of class III da neuron axon regeneration with regeneration percentage (B), regeneration index (C), and regeneration length (D).

(E) The genotypes of the animals and the temperature shift paradigm. n = 26–32 neurons from 4 to 6 larvae.

*$p < 0.05$, **$p < 0.01$ by Fisher's exact test (B) and two-tailed unpaired Student's t test (C and D). Scale bar, 20 μm.

See also Figure S3.

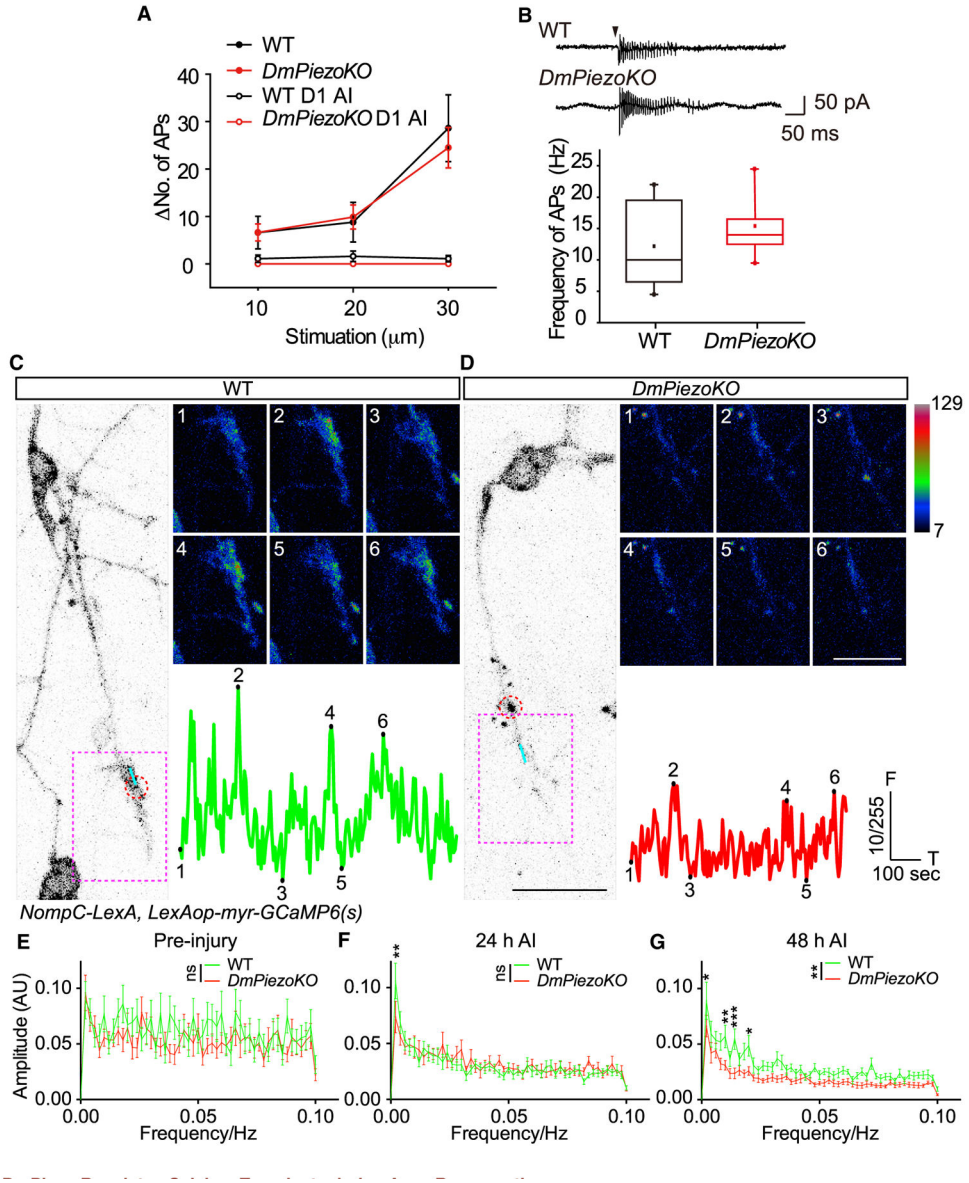

Figure 4. DmPiezo Regulates Calcium Transients during Axon Regeneration

(A) *DmPiezoKO* does not change the action potential (AP) firing of class III da neurons induced by displacements of the larval body wall. This mechanical response is largely abolished one day after injury (D1 AI) in both WT and *DmPiezoKO*. n = 5–10 neurons from 3 to 5 larvae.

(B) Axon injury triggers action potential firing in class III da neurons, and the firing frequency is comparable between WT and *DmPiezoKO*. n = 5–6 neurons from 4 to 5 larvae.

(C and D) At 48 hr AI, spontaneous calcium transients are present in the growth cones of WT larvae, but they are significantly reduced in *DmPiezoKO*. Calcium imaging was performed using membrane targeting myr-GCaMP6(s) in 3rd-instar larvae *in vivo*. For both WT (C) and *DmPiezoKO* (D), the neuronal cell body and the injured axon are shown on the left. The growth cone region (pink square) is zoomed in and six frames from the time-lapse

are shown. The red circle indicates the injury site and the blue line marks the region of interest (ROI) used for measuring fluorescence intensity. The raw calcium trace is shown with the six time points corresponding with the frames presented above.

(E–G) The amplitude of calcium transients in the growth cone is reduced in *DmPiezoKO* at 48 hr AI. The GCaMP fluorescence signal in each frame was subtracted and divided by the average fluorescence intensity of ROI in the 100 frames for each neuron, to normalize the baseline to 0. The fast Fourier transform (FFT) algorithm in MATLAB was then applied to decompose the fluorescence function of time into frequency components. The frequency domain representation of the original signal is shown by magnitude spectrum. The y axis indicates the relative amplitude of fluorescence vibration after FFT at specific frequency of the x axis. A statistical difference was observed only at 48 hr AI (G), but not pre-injury (E) or 24 hr AI (F). In particular, at 48 h AI, WT shows significantly higher amplitude at some low-frequency groups (0.002, 0.01, 0.014, 0.02 Hz) than those of *DmPiezoKO*. n = 17, 19, 17 neurons from 9, 10, 9 larvae for WT, and 22, 22, 16 neurons from 11, 11, 8 larvae for *DmPiezoKO* at pre-injury, 24 and 48 hr AI, respectively.

*p < 0.05, **p < 0.01, ***p < 0.001 by two-way ANOVA followed by Sidak's multiple comparisons test. Scale bar, 20 μm.

See also Figure S4.

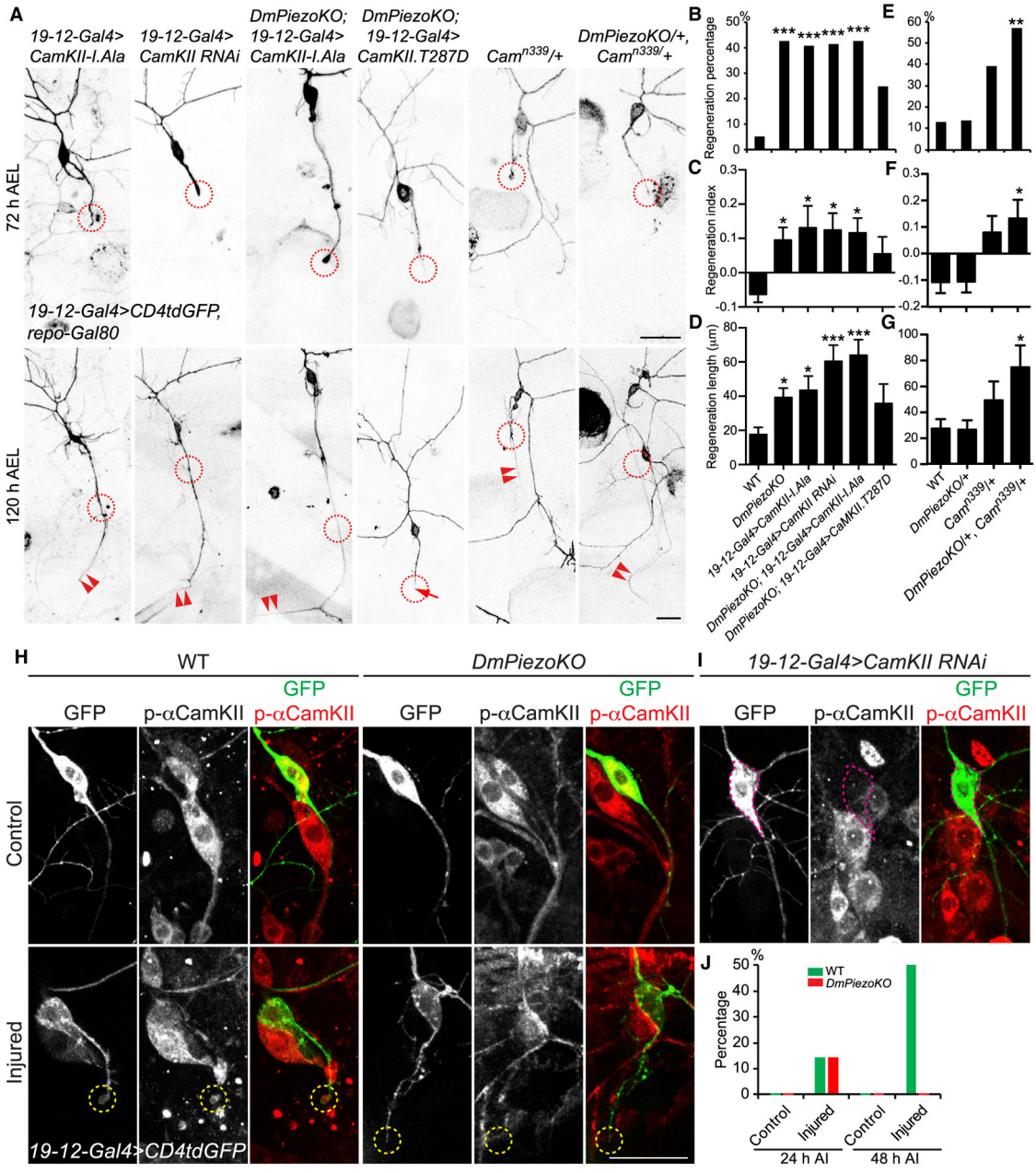

Figure 5. DmPiezo Functions through Calcium Signaling to Inhibit Axon Regeneration

(A) Inhibiting CamKII function with class III da neuron-specific expression of CamKII-I.Ala or CamKII RNAi promotes axon regeneration. CamKII-I.Ala over-expression in the *DmPiezoKO* background does not further enhance axon regeneration. Overexpression of the constitutively active CamKII-CamKII.T287D in DmPiezoKO attenuates the enhanced regeneration phenotype. While axon regeneration is slightly improved in $Cam^{n339/+}$ (a calmodulin-null allele) heterozygotes, transheterozygotes of $Cam^{n339/+}$ and *DmPiezoKO/+* significantly promote axon regeneration. The injury site is demarcated by the dashed circle, and arrowheads mark the regrowing axon tips.

(B–G) Quantification of class III da neuron axon regeneration with regeneration percentage (B and E), regeneration index (C and F), and regeneration length (D and G). n = 20–49 neurons from 5 to 16 larvae.

(H) In uninjured control, phosphor-CamKII (Thr^{305}) staining (p-αCamKII) is present diffusely in the class III da neuron cell body, axon, and dendrites, both in WT and *DmPiezoKO*. After injury, WT class III da neurons show enriched p-aCamKII staining in the growth cone tip (yellow dashed circle), which is not present in *DmPiezoKO*.

(I) CamKII RNAi in class III da neurons specifically abolishes the p-aCamKII staining in the cell body (magenta dashed circle), dendrites and axon.

(J) At 24 hr AI, a small fraction (14%) of the injured class III da neurons in WT or *DmPiezoKO* show p-aCamKII staining in the growth cone tip. However, at 48 h AI, whereas 50% of the WT class III da neurons show obvious staining in the growth cone tip, it is not present in *DmPiezoKO*. n = 4–8 neurons from 3 to 5 larvae. *$p < 0.05$, **$p < 0.01$, ***$p < 0.001$ by Fisher's exact test (B and E), one-way ANOVA followed by Dunnett's test (C, F, and G) or Dunn's test (D). Scale bar, 20 μm.

See also Figure S5.

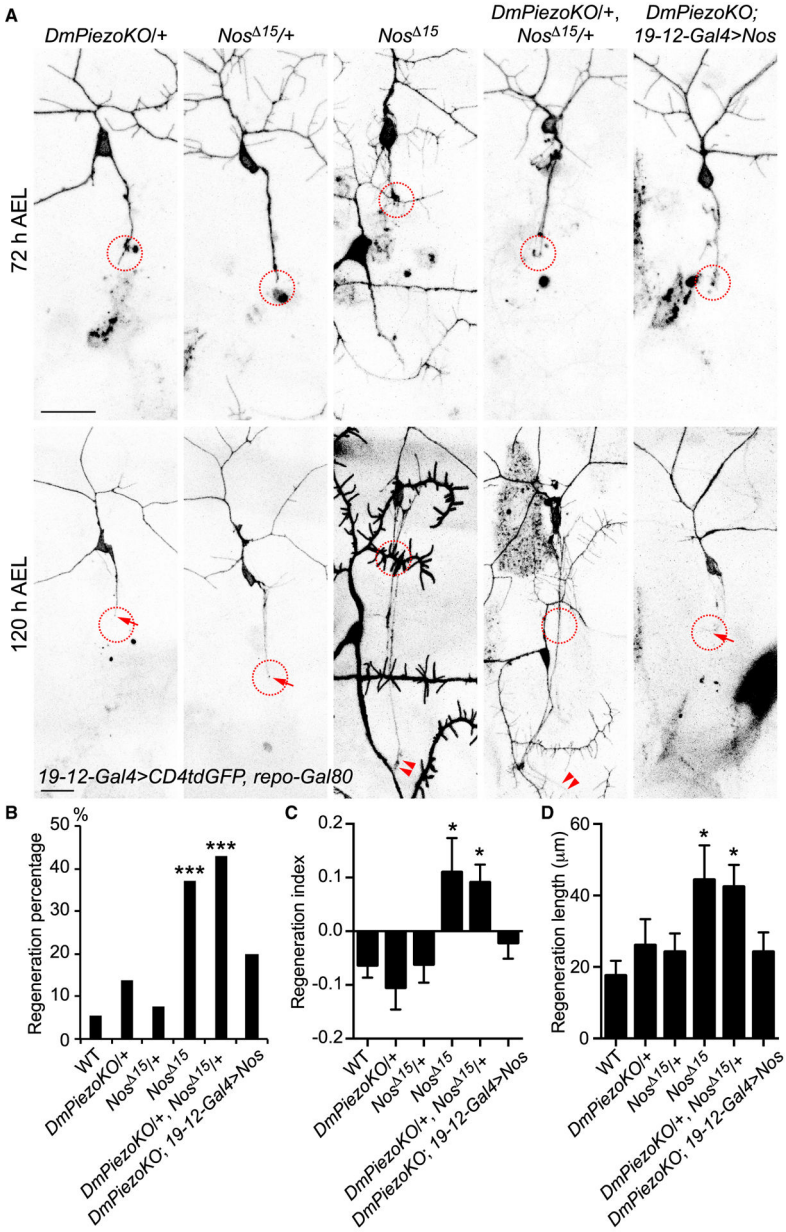

Figure 6. Nos Functions in Conjunction with DmPiezo to Inhibit Axon Regeneration

(A) Class III da neurons do not regrow in heterozygotes of *DmPiezoKO/+* or *Nos$^{\Delta 15}$/+*, whereas their regeneration is enhanced in the double transheterozygotes of *DmPiezoKO/+ Nos$^{\Delta 15}$/+*, and in *Nos$^{\Delta 15}$*. Class III da neuron-specific overexpression of Nos suppresses the enhanced regeneration phenotype in *DmPiezoKO*. The injury site is demarcated by the dashed circle. Arrow marks axon stalling, while arrowheads show the regrowing axon tips. (B–D) Quantification of class III da neuron axon regeneration with regeneration percentage (B), regeneration index (C), and regeneration length (D). n = 26–43 neurons from 7 to 10 larvae.

*p < 0.05, ***p < 0.001 by Fisher's exact test (B), one-way ANOVA followed by Holm-Sidak's test (C and D). Scale bar, 20 μm.

See also Figure S6.

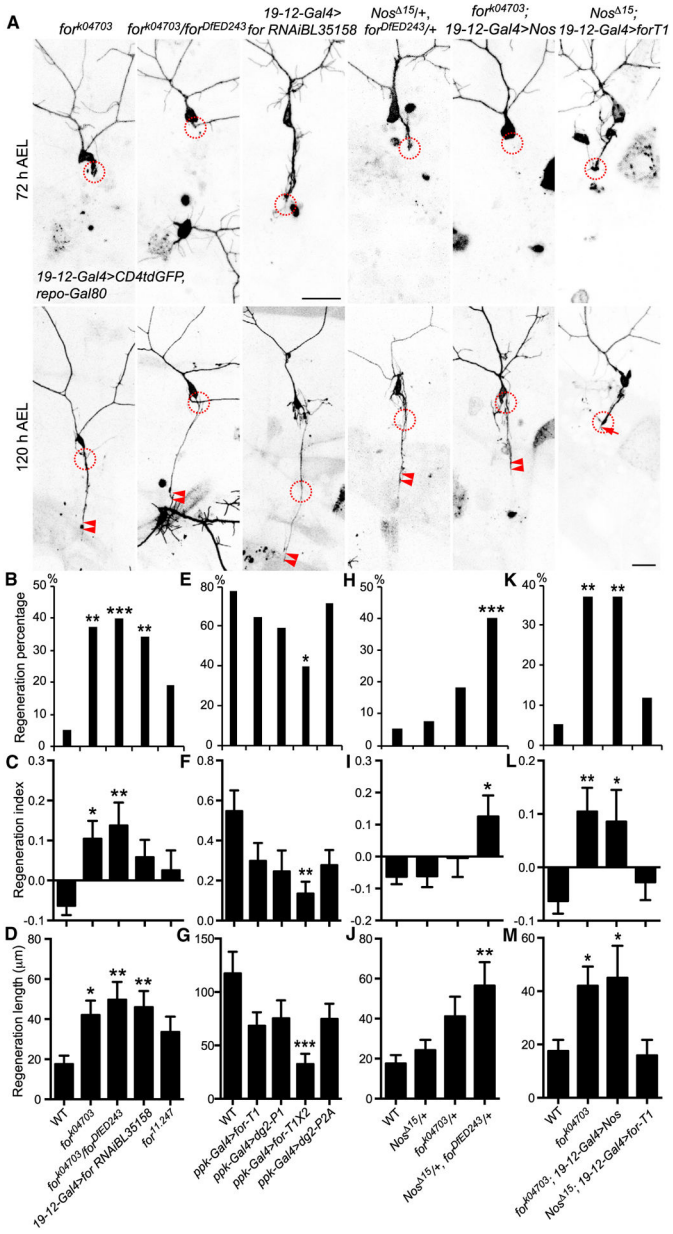

Figure 7. for or PKG Inhibits Axon Regeneration Downstream of Nos

(A) Class III da neuron axon regeneration is enhanced in for^{k04703}, transheterozygotes of for^{k04703}/ $for^{DfED243}$, class III da neuron-specific expression of *forRNAi*, double transheterozygotes of $Nos^{\Delta 15/+}$, $for^{DfED243/+}$, but not in $for^{11.247}$, heterozygotes of $Nos^{\Delta 15/+}$ or $for^{k04703/+}$. Class III da neuron-specific overexpression of Nos fails to mitigate the regeneration enhancement seen in $for^{k047037}$, whereas FOR-T1 over-expression largely suppresses the phenotype in $Nos^{\Delta 15}$.

(B–M) Quantification of class III da neuron axon regeneration with regeneration percentage (B, H, and K), regeneration index (C, I, and L), and regeneration length (D, J, and M). Quantification of class IV da neuron axon regeneration with regeneration percentage (E), regeneration index (F), and regeneration length (G). Whereas expressing a single copy of

FOR-T1 with two independent alleles: *for-T1* and *dg2-P1* or FOR-T2 with *dg2-P2A* all fail to achieve significant inhibition in class IV da neurons, overexpressing two copies of FOR-T1 (*for-T1X2*) impedes axon regeneration. n = 17–37 neurons from 5 to 15 larvae. *p < 0.05, **p < 0.01, ***p < 0.001 by Fisher's exact test (B, E, H, and K), one-way ANOVA followed by Holm-Sidak's test (C and F), Dunn's test (D), or Dunnett's test (G, I, J, L, and M). Scale bar, 20 μm.

See also Figure S7.

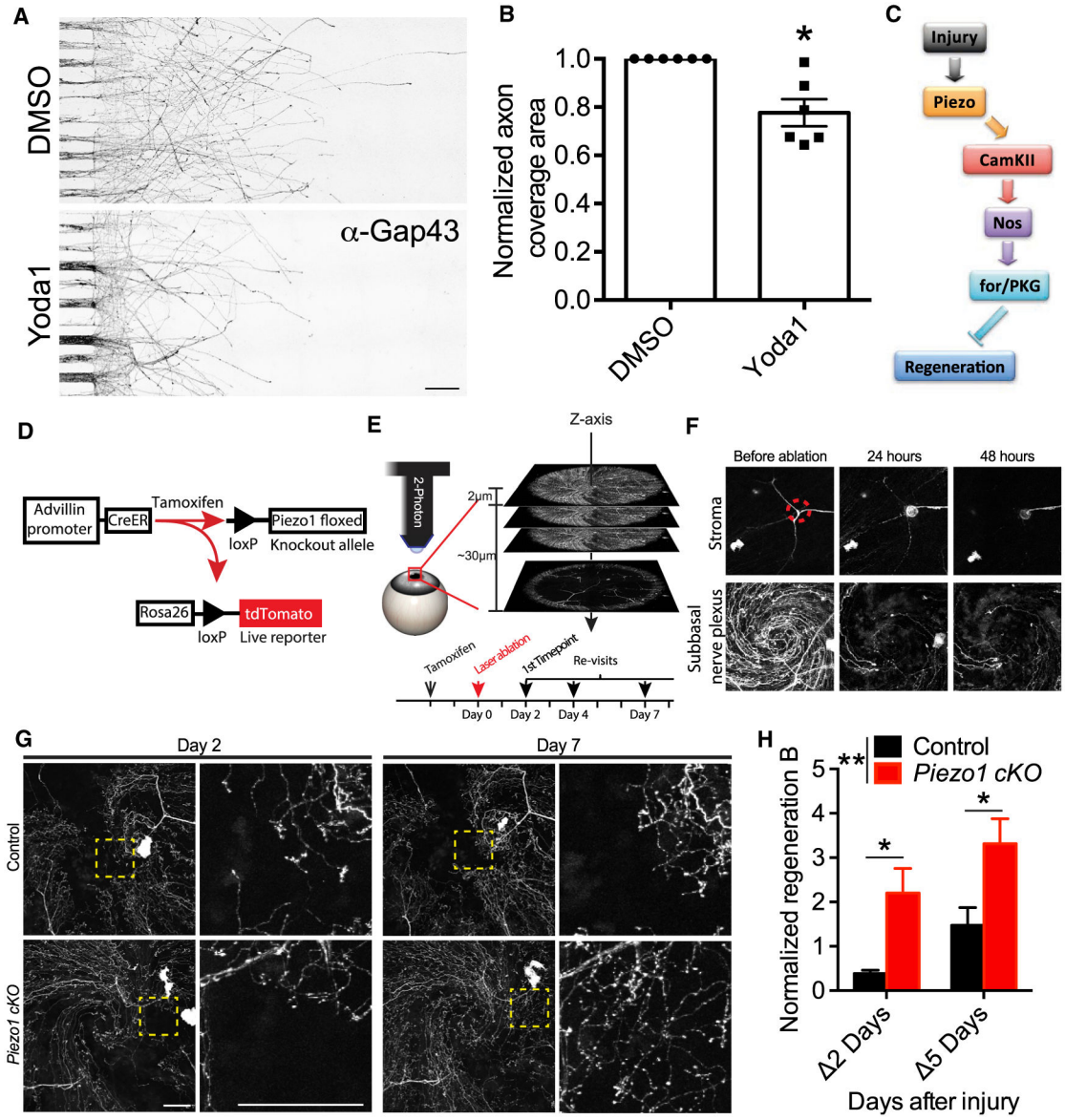

Figure 8. Piezo Inhibits Axon Regeneration in Mammalian Injury Models

(A) Piezo1 agonist Yoda1 (30 μM) modestly reduces axon regeneration of rat hippocampal neurons cultured in a microfluidic chamber, when applied to the axon terminal chamber immediately after injury. The axons are labeled with α-Gap43 staining.

(B) The axon coverage area is measured and normalized to the total width of the microgrooves. The value from the Yoda1 group is further normalized to the corresponding DMSO vehicle control group in the same experiment. Yoda1 treatment modestly reduces the coverage area of the regrown axons. n = 6 experiments.

(C) The proposed Piezo-CamKII-Nos-for or PKG signaling cascade that responds to injury and inhibits axon regeneration.

(D) To label corneal sensory axons and generate sensory neuron-specific Piezo1 conditional knockout (*Piezo1 cKO*), mice are bred with *Advillin(Avil)-CreER; Rosa-stop-tdTomato;*

Piezo1$^{fl/fl}$ alleles, and Cre-mediated recombination is induced by tamoxifen (TAM) injection.

(E) A 2-photon microscopy based intravital imaging system is implemented to visualize and manipulate tdTomato-labeled corneal sensory nerves in live mice. Serial optical sections are collected to reconstitute a max-projection image of the entire cornea. The timeline describes the experimental paradigm, including tamoxifen injection, laser ablation, nerve ablation, and imaging.

(F) The larger nerve trunks located in the stroma are ablated before they branch into thinner fibers (dashed circle). The degeneration of the nerve fibers downstream of the ablation sites both in the stroma and the subbasal nerve plexus is confirmed by imaging at 24 and 48 hr after ablation.

(G) In the control group (normal siblings, *Avil-CreER; Piezo1*$^{fl/+}$ + TAM), corneal sensory axons show limited regeneration within 7 days post-ablation, leaving large areas deprived of sensory innervation. *Piezo1 cKO* (*Avil-CreER; Piezo1*$^{fl/fl}$ + TAM) show accelerated axon regeneration, with more vacant space reinnervated by the regenerating nerve fibers.

(H) The regenerating axons are manually traced and the length of regrown axons is measured. *Piezo1 cKO* exhibits significantly higher regeneration capacity as reflected by the increase of the total length of regenerating nerve fibers. The dataset for normalized regeneration B is shown. n = 4 mice for control and 5 mice for *Piezo1 cKO*.

*p < 0.05, **p < 0.01 by two-tailed unpaired Student's t test (B), two-way ANOVA followed by Sidak's multiple comparisons test (H). Scale bar, 100 μm.

See also Figure S8.

KEY RESOURCES TABLE

REAGENT or RESOURCE	SOURCE	IDENTIFIER
Antibodies		
mouse anti-Fasciclin II	DSHB	Cat# 1D4; RRID:AB_528235
rabbit anti-Gap43	Novus Biologicals	Cat# NB300–143; RRID:AB_10001196
mouse anti-MAP2	Sigma	Cat# M9942; RRID:AB_477256
rabbit anti-phospho-CaMKII alpha/beta/delta (Thr305)	Thermo Fisher Scientific	Cat# PA5–37832; RRID:AB_2554440
Bacterial and Virus Strains		
plasmid: mPiezo1-pcDNA3.1-IRESgfp	Coste et al., 2015	N/A
plasmid: mPiezo1–2336-Myc	Coste et al., 2015	N/A
plasmid: mPiezo1-TriM	Coste et al., 2015	N/A
plasmid: hPiezo1-pIRES2-EGFP	Coste et al., 2015	N/A
plasmid: UAS-mPiezo1	This paper	N/A
plasmid: UAS-mPiezo1–2336-Myc	This paper	N/A
plasmid: UAS-mPiezo1-TriM	This paper	N/A
plasmid: UAS-hPiezo1	This paper	N/A
Chemicals, Peptides, and Recombinant Proteins		
negative tone photoresist formulations 2–25	MicroChem	Cat# SU-8
permanent epoxy negative photoresist	MicroChem	Cat# SU-8 2150
Polydimethylsiloxane	Dow Corning	Cat# Sylgard 184
Yoda	Sigma	Cat# SML1558
Tamoxifen	Sigma	Cat# T5648
Critical Commercial Assays		
Quick-RNA MiniPrep Plus Kit	Zymo Research	Cat# R1058
Experimental Models: Organisms/Strains		
D. melanogaster. 19–12-Gal4	Xiang et al., 2010	N/A
D. melanogaster. reop-Gal80	Awasaki et al., 2008	N/A
D. melanogaster. DmPiezoKO	Kim et al., 2012	N/A
D. melanogaster. UAS-DmPiezoRNAiv2796	Kim et al., 2012	N/A
D. melanogaster. DmPiezo-Gal4	Kim et al., 2012	N/A
D. melanogaster. ppk-CD4-tdGFP	Han et al., 2011	N/A

REAGENT or RESOURCE	SOURCE	IDENTIFIER
D. melanogaster. ppk-Gal4	Han et al., 2011	N/A
D. melanogaster. NompC-QF	Petersen and Stowers, 2011	N/A
D. melanogaster: QUAS-mCD8GFP	Potter et al., 2010	N/A
D. melanogaster. QUAS-mtdTomato	Potter et al., 2010	N/A
D. melanogaster. UAS-CD4TdTomato	Han et al., 2011	N/A
D. melanogaster: UAS-CamKII-I.Ala	Joiner and Griffith, 1997	N/A
D. melanogaster. UAS-CamKII RNAi	Ashraf et al., 2006	N/A
D. melanogaster. UAS-CamKII.T287D	Jin etal., 1998	N/A
D. melanogaster. Nos^{A15}	Yakubovich et al., 2010	N/A
D. melanogaster. Nos^{1}	Lacin et al., 2014	N/A
D. melanogaster. UAS-Nos	Lacin et al., 2014	N/A
D. melanogaster. for^{k04703}	Spradling et al., 1999	N/A
D. melanogaster. $for^{11.247}$	Eddison et al., 2012	N/A
D. melanogaster. UAS-for-T1	Belay et al., 2007	N/A
D. melanogaster. UAS-dg2-P1	MacPherson et al., 2004	N/A
D. melanogaster. UAS-dg2-P2A	MacPherson et al., 2004	N/A
D. melanogaster: hsFLP;;UAS > CD2 > mCD8-GFP	Grueber et al., 2007	N/A
D. melanogaster: m12-Gal4 (P(Gal4)tey^{5053A}*)*	Ritzenthaler et al., 2000	N/A
D. melanogaster. UAS-GCaMP6s	Chen et al., 2013	N/A
D. melanogaster. Cam^{n339}	Heimanet al., 1996	N/A
D. melanogaster. NompC-LexA	Shearin et al., 2013	N/A
D. melanogaster. tub-Gal80^{ts}	McGuire et al., 2003	N/A
D. melanogaster. UAS-Dcr-2	Bloomington Drosophila Stock Center	N/A
D. melanogaster. $for^{DfED243}$	Bloomington Drosophila Stock Center	N/A
D. melanogaster. UAS-forRNAiBL35158	Bloomington Drosophila Stock Center	N/A
D. melanogaster. LexAop-myr-GCaMP6(s)	Freeman lab	N/A
D. melanogaster. UAS-mPiezo1	This paper	N/A
D. melanogaster. UAS-hPiezo1	This paper	N/A
D. melanogaster. UAS-mPiezo1–2336-Myc	This paper	N/A
D. melanogaster. UAS-mPiezo1-TriM	This paper	N/A
Mouse: Advillin-CreER	Lau et al., 2011	RRID:IMSR_JAX:032027

REAGENT or RESOURCE	SOURCE	IDENTIFIER
Mouse: *Piezo1*$^{fl/fl}$	Cahalan et al., 2015	RRID:IMSR_JAX:029213
Mouse: Rosa-stop-tdTomato	Madisen et al., 2010	RRID:IMSR_JAX:007905
Oligonucleotides		
for F1 primer: gtcgggtcagaatttccaga	This paper	N/A
for F2 primer: cagaggattcccaggatcaa	This paper	N/A
for F3 primer: ggaaaagtgcgagtgacgat	This paper	N/A
for R primer: agtttggaccagotctacgc	This paper	N/A
α-tubulin forward primer: *acaacgaggctatctacgaca*	This paper	N/A
α-tubulin reverse primer: ttttcagtgttgcagtgaattt	This paper	N/A
Recombinant DNA		
plasmid: mPiezo1-pcDNA3.1-IRESgfp	Coste et al., 2015	N/A
plasmid: mPiezo1–2336-Myc	Coste et al., 2015	N/A
plasmid: mPiezo1-TriM	Coste et al., 2015	N/A
plasmid: hPiezo1-plRES2-EGFP	Coste et al., 2015	N/A
plasmid: UAS-mPiezo1	This paper	N/A
plasmid: UAS-mPiezo1–2336-Myc	This paper	N/A
plasmid: UAS-mPiezo1-TriM	This paper	N/A
plasmid: UAS-hPiezo1	This paper	N/A
Software and Algorithms		
GraphPad Prism 6	GraphPad Software	N/A
ImageJ	https://imagej.nih.gov/ij/	N/A
Zen	Zeiss	N/A
LAX	Leica	N/A
Olympus Viewer	Olympus	N/A
pClamp9	Molecular Devices	N/A
MATLAB	MathWorks	N/A